RESIDUE NUMBER SYSTEM ARITHMETIC INSPIRED APPLICATIONS IN CELLULAR DOWNLINK OFDMA

by

DALIN ZHU

B.Eng., Beijing University of Posts and Telecom., China, 2007

A THESIS

submitted in partial fulfillment of the

requirements for the degree

MASTER OF SCIENCE

Department of Electrical and Computer Engineering

College of Engineering

KANSAS STATE UNIVERSITY

Manhattan, Kansas

2009

Approved by:

Major Professor

Balasubramaniam Natarajan

Copyright

Abstract

In recent years, orthogonal frequency division multiplexing (OFDM) scheme has received significant research interest due to its capability of supporting high data rates in hostile environments. As compared to conventional single-carrier modulation schemes, OFDM benefits from low complexity equalization filters and high spectral efficiency. A multiple access implementation of OFDM, i.e., orthogonal frequency division multiple access (OFDMA) has been considered as the multiple access (MA) scheme in 3GPP LTE, or LTE advanced downlink. In cellular OFDMA, frequency hopping (FH) is widely used to exploit frequency diversity gain and improve system throughput; and pilot patterns that have low-cross correlation are employed to improve the quality of channel estimation. However, there are numerous unsolved problems that need to be addressed in frequency hopped and pilot assisted OFDMA systems.

Surveying the prior works in the literature, we find that limited research efforts have focused on coping with the inherent disadvantages regarding OFDM in cellular OFDMA systems. In this thesis, we employ the so-called residue number system (RNS) arithmetic concentrating on (a) FH pattern design for minimizing/averaging intra/inter-cell interference, (b) pilot pattern design for improving the quality of channel estimation, and (c) pilot pattern design for facilitating time-frequency synchronization and device identification in multi-cell OFDMA. Regarding (a), RNS-based FH patterns not only preserve orthogonality within the same cell, but also have the minimum number of symbol collisions among adjacent cells. Additionally, the RNS-based method exhibits consistent system performance and more frequency diversity gains as compared to previous efforts. With respect to (b), RNS-based pilot pattern design generates more unique pilot patterns than conventional

methods. This results in low probability of pilot-to-pilot collisions, which in turn, significantly improves the quality of channel estimation from the system level perspective. For (c), as a special case of linear congruence sequences, RNS-based pilot patterns have good auto-correlation properties, which are extremely helpful in time-frequency synchronization and device identification.

Table of Contents

Table of Contents v

List of Figures vii

List of Tables ix

Acknowledgements x

1 Introduction 1

1.1 OFDM/OFDMA . . . 2

1.1.1 Peak-to-average Power Ratio . . . 4

1.1.2 Time and Frequency Synchronization . . . 4

1.1.3 Coherent Detection and Estimation . . . 5

1.1.4 Intra/inter-cell Interference . . . 7

1.2 Frequency Hopping Patterns . . . 8

1.3 Pilot Hopping Patterns . . . 10

1.4 Motivation and Contributions . . . 10

1.4.1 Motivation . . . 10

1.4.2 Contributions . . . 12

1.5 Organization . . . 13

2 Residue Number System Arithmetic 14

2.1 Conventional Number System . . . 14

2.2 Residue Number System . . . 15

2.2.1 Residue Number System Transform and Its Inverse . . . 16

2.2.2 Properties of Residue Number System . . . 17

2.3 Summary 19

3 RNS aided FH Pattern Design in Downlink OFDMA 21

3.1 System Model of Coded Frequency-Hopped OFDMA 21

3.1.1 Signal Transmission Scheme 22

3.1.2 Access Model 24

3.1.3 Interference Model 26

3.2 RNS-FH Pattern Design 28

3.3 Simulation Results 34

3.4 Summery 40

4 RNS aided Pilot Pattern Design in Downlink OFDMA 44

4.1 System Model 44

4.2 RNS-pilot Pattern Design 46

4.3 Simulation Results 50

4.4 Summary 54

5 Conclusions and Future Work 55

5.1 Conclusions 55

5.2 Future Work 56

Bibliography 58

Bibliography 63

List of Figures

1.1 Block diagram of an OFDM transceiver 2
1.2 Example of band division in downlink OFDMA 3
1.3 Block diagram of OFDM receiver with coherent detection 5
1.4 Example of pilots in a block of 15 OFDM symbols with 13 subcarriers 6
1.5 Illustrative example of intra and inter-cell interference in cellular cells 7
1.6 Example of the time-frequency grid with six hopping users, a - g 9

3.1 The block diagram of coded FH-OFDMA system. 22
3.2 One example of RNS assisted two-stage hopping strategy. 32
3.3 One example of RNS assisted multi-stage hopping strategy. 33
3.4 Two different FH patterns are given and their only collision point is highlighted. 34
3.5 Channel correlation function. 36
3.6 Expected number of collisions per symbol versus the number of users. 37
3.7 BER vs. SNR of RNS-FH OFDMA under cluster and independent hopping with different channel conditions. N=110, M=M_c=10, N_c=11, f_DT_s=0.01. . 38
3.8 Inter-cell interference-to-signal power ratio for given users under different RNS-FH patterns and identical RNS-FH patterns assignments across cells . . 39
3.9 BER vs. SIR of RNS-FH OFDMA under cluster hopping with different channel conditions. N=110, M=M_c=10, N_c=11, SNR = 25dB, f_DT_s=0.01. . . . 40
3.10 BER vs. SIR of RNS-FH OFDMA under independent hopping with different channel conditions. N=110, M=M_c=10, N_c=11, SNR = 25dB, f_DT_s=0.01. . 41
3.11 BER vs. user loads of RNS-FH OFDMA under cluster hopping with different channel conditions, N=110, M=M_c=10, N_c=11, SNR = 25dB, SIR = 15dB, f_DT_s=0.01. 42

3.12 BER vs. user loads of RNS-FH OFDMA under independent hopping with different channel conditions, N=110, M=M_c=10, N_c=11, SNR = 25dB, SIR = 15dB, f_DT_s=0.01. 42
3.13 Performance of cluster-hopped RNS-FH OFDMA with different cluster sizes and different number of active users, f_DT_s=0.01. 43
3.14 Performance of independent-hopped RNS-FH OFDMA vs. LS-FH OFDMA, N=110, M=M_c=10, N_c=11, LS A_4 and A_{38} are used, different moduli sets $m_1 = \{2, 55\}$ and $m_2 = \{2, 11, 5\}$ are applied to construct RNS-FH patterns, f_DT_s=0.01. 43

4.1 Block diagram of MIMO-OFDMA system within a single cell 44
4.2 Proposed RNS-based pilot pattern 49
4.3 SER performance of regular and RNS-based pilot pattern assisted channel estimation in a link level simulation, ρ=0dB 51
4.4 MSEs of regular and RNS-based pilot pattern assisted channel estimation in a link level simulation, ρ=0dB 52
4.5 System throughput of RNS-based pilot pattern assisted channel estimation in a system level simulation, SNR=20dB, SIR=15dB, ρ=0dB, 25% pilot density 53

List of Tables

2.1 RNS representation of the integer N_k 16

3.1 System Parameters of frequency hopped OFDMA 35

4.1 System Parameters of pilot assisted OFDMA 50

4.2 Number of unique pilot patterns 52

Acknowledgments

I would like to express my sincere gratitude to my graduate advisor, Dr. Bala Natarajan for his support, encouragement, and friendship. It is my honor to have the chance to work with him, and I believe this experience would be my most memorable time in my life. He not only has wonderful insights into academics that I can learn from, but also owns great personalities that I am sure to cherish for the rest of my journey. His fruitful discussions and valuable suggestions would benefit the rest of my life, no matter where I will be. I would like to extend my sincere gratitude to Dr. Don Gruenbacher and Dr. William B. Kuhn for agreeing to serve as my committee members, reviewing my thesis and providing insightful suggestions. It was enjoyable to work in WiCom group. I would like to thank my former and current colleges for their support, encouragement, and friendship as well.

Finally, I dedicate all my work to my mom who dedicates all her life to me.

Chapter 1

Introduction

The spectacular growth of data communication over wireless environments demands reliable and efficient transmission schemes. In contrast to conventional serial modem schemes, multi-carrier modulation (MCM) has received widespread attention in both academics and industries due to its ability to cope with severe channel conditions. Orthogonal Frequency Division Multiplexing (OFDM) is a form of MCM, where a large number of orthogonal subcarriers are employed to carry data. The first OFDM scheme was proposed in 1966 by Chang [1], and widely investigated in 1990s. The system's operational principle is that a high-rate wide band transmission is divided into a large number of low-rate narrow band transmissions. In this way, the mobile channel can be considered as non-dispersive channel, which in turn, significantly simplifies receiver design. In addition, OFDM forms the foundation of a multiple access (MA) scheme, termed as orthogonal frequency division multiple access (OFDMA). In OFDMA, multiple access is realized by providing each user with a fraction of all available subcarriers. In contrast to conventional FDMA scheme, OFDMA avoids the relatively large number of guard bands that are necessary for separating different users. However, OFDM/OFDMA also has inherent difficulties such as high peak-to-average power ratio (PAPR), time-frequency offsets, channel estimation errors, and inter/intra-cell interference. In the following sections, detailed descriptions of OFDM/OFDMA are presented.

Relative challenges in this research area are given as well, associated with suggestions on how to cope with these drawbacks.

1.1 OFDM/OFDMA

The basic principle of OFDM is to divide a high-rate data stream into a number of parallel lower-rate streams that are transmitted on orthogonal subcarriers (frequencies). In this way, the symbol duration increases which in turn, reduces the amount of dispersion in time that is caused by multipath delay spread. In addition, guard interval is introduced in every OFDM symbol duration in order to eliminate inter-symbol interference (ISI). In the guard interval, the OFDM symbol is cyclically extended to avoid inter-carrier interference (ICI). It has been shown that [2] the complex baseband OFDM signal is in fact the inverse discrete Fourier transform (IDFT) of input symbols. In practice, this transform can be implemented by the inverse fast Fourier transform (IFFT), which reduces the number of complex arithmetic operations. The block diagram of an OFDM transceiver is given in Fig.1.1.

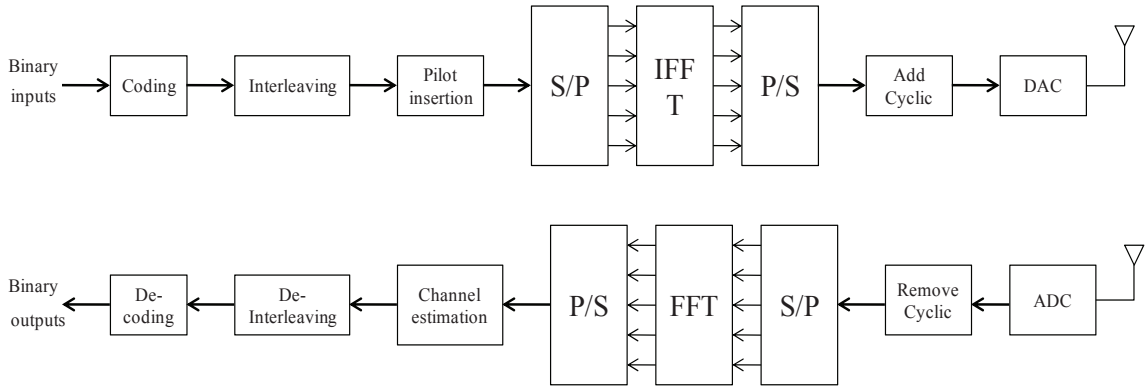

Figure 1.1: *Block diagram of an OFDM transceiver*

For a N-point IFFT, one OFDM symbol can be written as

$$s(n) = \sum_{i=0}^{N_s-1} x_i \exp(j2\pi \frac{in}{N}), \tag{1.1}$$

where x_i are complex symbols, N_s is the total number of subcarriers, and n represents one sample number.

Orthogonal Frequency Division Multiple Access (OFDMA) is a multi-user version of OFDM modulation scheme. Multiple access is achieved in OFDMA by assigning subsets of subcarriers to individual users. This allows simultaneous low data rate transmissions from different users. In contrast to conventional FDMA scheme, OFDMA benefits from averaging inter/intra-cell interference by using different basic carrier permutations between users. Therefore, OFDMA is used in WiMAX, IEEE 802.20, and being considered in the downlink 3GPP Long Term Evolution (LTE) fourth generation mobile broadband standard. One illustrative example of downlink OFDMA is given in Fig.1.2. Readers are referred to [3] for details in OFDMA standardization.

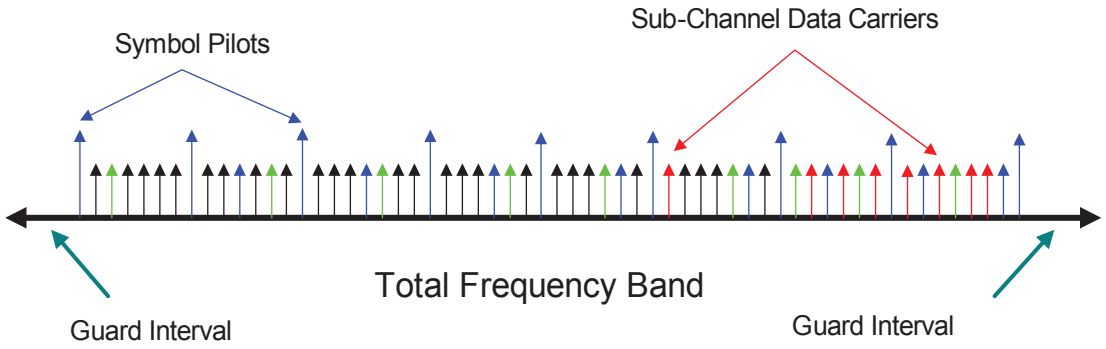

Figure 1.2: *Example of band division in downlink OFDMA*

Although OFDM/OFDMA modulation schemes can alleviate the problem of multipath propagation in mobile wireless channels, inherent disadvantages regarding OFDM/OFDMA, namely high peak-to-average power ratio (PAPR), time-frequency offsets, channel estimation errors and intra/inter cell interference still need to be addressed. In following parts, detailed descriptions of above mentioned inherent difficulties are presented, along with suggestions on how to cope with them.

1.1.1 Peak-to-average Power Ratio

The OFDM signal in equation 1.1 is in fact the superposition of a large number of modulated complex signals - this may result in a high instantaneous signal peak relative to the average signal level. However, practical amplifiers usually exhibit a finite amplitude range, in which they can be considered as almost linear. Therefore, if an OFDM signal has high peak-to-average power ratio, the time domain signal traverses from a low instantaneous power waveform to a high power waveform, resulting in high out-of-band distortion power [4]. In order to avoid saturating the RF amplifier, several techniques have been proposed for reducing PAPR. Specifically, these techniques can be divided into three categories. The first category simply reduces the peak power by nonlinearly distorting OFDM signals [5]. However, the main drawback of peak cancelation technique is that symbols with a large PAPR suffer from more degradation, which in turn, results in more vulnerable errors. The second category is coding technique that basically uses a special set of error correcting codes that exclude OFDM symbols with high PAPR. Representative works in this category can be addressed to [6][7][8]. The third category employs different algorithms for post-processing the time domain OFDM signal prior to amplification [9][10][11]. A more comprehensive overview of PAPR reduction techniques can be addressed to [12].

1.1.2 Time and Frequency Synchronization

Another disadvantage of OFDM modulation scheme is the issue of time-frequency offsets. Theoretically, OFDM subcarriers are perfectly orthogonal if and only if the transmitter and receiver use exactly the same frequencies. However, in practice, oscillator does not produce a carrier at exactly one frequency, but rather a carrier that is modulated by random phase jitter. Therefore, the frequency is never perfectly constant, resulting in inter-carrier interference (ICI) in an OFDM receiver. In addition, OFDM signals suffer from time-offset as well, which reduces the robustness of delay spread. However, comparing with frequency offset, OFDM is relatively more robust to time offset. A wide variety of techniques have been

proposed to estimate and correct time-frequency offsets at the OFDM receiver. Basically, OFDM time-frequency synchronization techniques can be divided into two categories. They are: (1) fine time and frequency tracking algorithms exploiting the OFDM signal's cyclic extension [13][14]; (2) rough time and frequency acquisition algorithms relying on known pilot symbols embedded into OFDM symbols [15][16][13].

1.1.3 Coherent Detection and Estimation

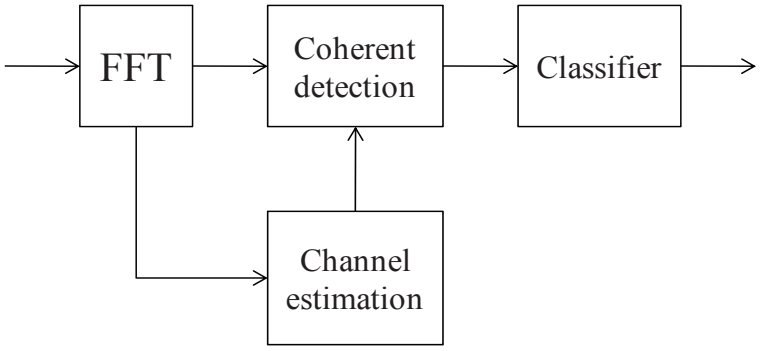

Figure 1.3: *Block diagram of OFDM receiver with coherent detection*

In OFDM modulation scheme, binary bits are modulated on OFDM subcarriers and transmitted via wireless channels. Hence, at the receiver, in order to fully recover the original information, or facilitate coherent detection, channel state information (CSI) is required. The block diagram of OFDM receiver with coherent detection is given in Fig.1.4. The task of the channel estimation block is to learn instantaneous channel conditions, such that all received symbols can be converted to binary soft decisions via coherent detection block. One popular way to acquire CSI at the receiver is the so-called pilot-aided channel estimation. In pilot-aided transmission (PAT) scheme, known signals (referred to as pilots) are embedded in OFDM symbols across time and frequency. At the receiver, estimates of these known signals are used to determine the best possible decision boundaries for the constellation of each subcarrier. In PAT scheme, the main issue is to determine how to place

pilots across time and frequency domains, without introducing too much training overhead and avoiding severe aliasing.

It is well known that wireless channel fades in both time and frequency. Therefore, in order to fully reconstruct channel's response, pilot signals are inserted into both time and frequency domains, namely two-dimensional channel estimator. This concept can be clearly revealed in Fig.1.4. In Fig.1.4, there are 15 OFDM symbols, with 13 subcarriers in each

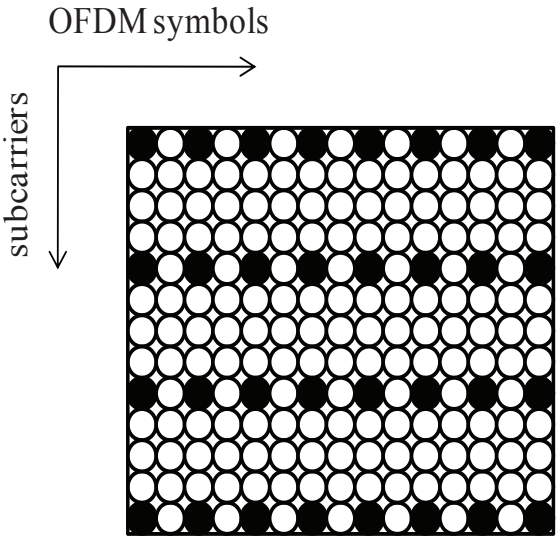

Figure 1.4: *Example of pilots in a block of 15 OFDM symbols with 13 subcarriers*

symbol. Black circle values are referred to as pilots. From the standpoint of sampling theory, in order to fully interpolate channel's response in both time and frequency, the pilot spacing has to fulfill the Nyquist sampling theorem. That is, in the context of OFDM, there exist both a minimum subcarrier spacing and a minimum symbol spacing between pilots. These spacings between pilot signals are determined by the bandwidth of the channel variations in time and frequency, which correspond to the maximum Doppler spread $\nu_{\max}$ and maximum delay spread $\tau_{\max}$, respectively. Mathematically, the requirements for the spacings between pilots in time and frequency (T_p and f_p, respectively) can be expressed as,

$$T_p < \frac{1}{\nu_{\max}}, \tag{1.2}$$

$$f_p < \frac{1}{\tau_{\max}}. \tag{1.3}$$

Other OFDM channel estimation techniques are reviewed in [12]. Readers are referred to [4] for detailed descriptions.

1.1.4 Intra/inter-cell Interference

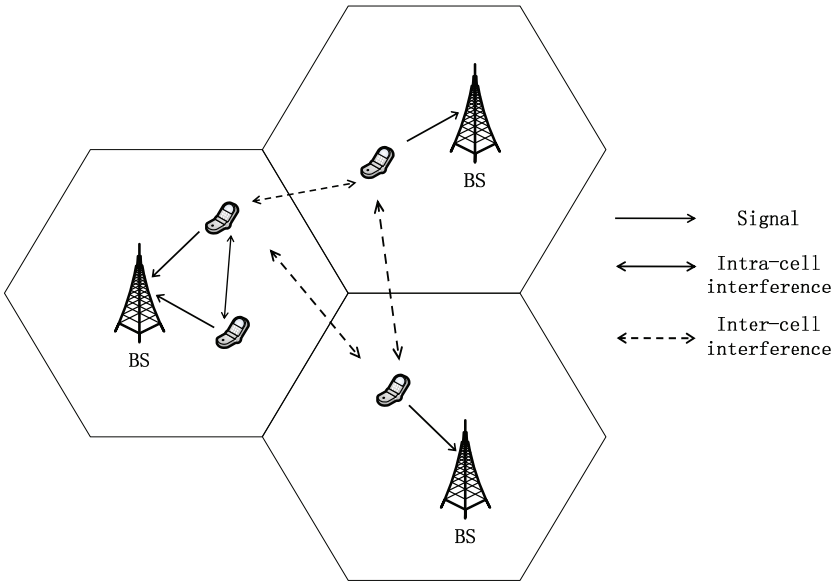

Figure 1.5: *Illustrative example of intra and inter-cell interference in cellular cells*

In cellular OFDMA, interference management is critical. From a system level perspective, the same set of frequencies can be reused by multiple base stations (BSs), as long as they are physically separated far enough. Base stations that use the same frequency band give a rise to co-channel interference. Co-channel interference occurs within the same cell, or among adjacent cells. Typically, co-channel interference in cellular downlink OFDMA is divided into two categories, which are intra-cell interference and inter-cell interference, respectively. One example illustrating intra-cell and inter-cell interference in a cellular environment is given in Fig.1.5. For conventional cellular system, frequency reuse or frequency planing is employed to coordinate the co-channel interference and make intelligent radio

resource allocation over base stations [17][18]. However, challenges remain when applying typical frequency planing scheme to OFDMA cellular systems. 3GPP LTE suggests the use of different basic carrier permutations between users (i.e., frequency hopping) to average intra/inter-cell interference. This aspect is discussed in the following part.

1.2 Frequency Hopping Patterns

In conventional OFDMA, each user is assigned a fixed set of subcarriers for transmitting information symbols. If hopping of subcarriers per time slot (OFDM symbol) is allowed, the system benefits from increased frequency diversity, along with minimized intra-cell interference, and averaged inter-cell interference. In addition, by using forward-error correction (FEC) coding over multiple hops, the system can correct for subcarriers in deep fades, or subcarriers that are interfered by other users. Such a transmission scheme is referred to as frequency hopped OFDMA, and hopping sequences of each user in both time and frequency form frequency hopping (FH) patterns. One illustrative example of orthogonal FH pattern is given in Fig.1.6. Here, six users (a - g) access the system. Each user hops to a different frequency for transmitting within each OFDM symbol duration. Additionally, there is zero collision among users over the entire six time slots.

It is desirable for FH pattern design to satisfy the following conditions [19]: (i) minimize intra-cell interference; (ii) average inter-cell interference; (iii) avoid ambiguity while identifying users, and (iv) exploit frequency diversity by forcing hops to span a large bandwidth. The first aspect is relatively easy to achieve by using orthogonal hopping patterns within a cell. To average inter-cell interferences, hopping patterns are constructed in a way that two users in different cells interfere with each other only during a small fraction of all hops. The third condition requires base stations to have the capability of distinguishing different users efficiently according to their unique FH signatures. Finally, the last requirement not only ensures the security of the transmission, but also mitigates the effect of fading by exploiting frequency diversity.

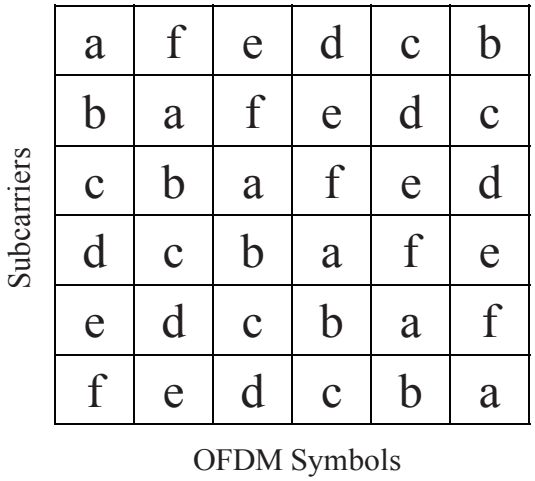

Figure 1.6: *Example of the time-frequency grid with six hopping users, a - g*

Frequency hopping pattern design has received considerable attention in both commercial and military communication systems. There has been extensive work on designing FH-OFDMA systems. In [20], concepts of fast frequency hopping along with OFDM are illustrated. In [21], authors show that the expected number of collisions per symbol under both independent and cluster hopping does not depend on the hopping strategy. In their later work [22], it is shown that the number of collisions can be further reduced by using space-frequency coding in multiple-antenna systems. Orthogonal Latin Squares (LS) are presented as FH patterns in TCM/BICM coded OFDMA in [23]. In LS aided FH-OFDMA systems, it is seen that there is a wide variability in the performance of users in different cells. Therefore, it is not an effective scheme if one considers fairness to be important. Welch-Costas array is introduced in [24] and evaluated in [25] for coded FH-OFDMA. Here, although users across cells experience significant performance improvements, users within a cell may not occupy all of the available bandwidth to exploit full frequency diversity. Other aspects focusing on preventing hostile jamming and pilot assisted channel estimation in FH-OFDMA are explored in [26] and [27], respectively.

1.3 Pilot Hopping Patterns

Theoretically, there is no significant difference in pilot aided channel estimation between downlink OFDMA and conventional single user OFDM. In OFDMA, pilot signals are assigned to different access users according to their rate requirements, as well as the entire system budget. From the system level perspective, different pilot patterns have to be allocated to different base stations while minimizing the number of collisions among the patterns. This is because if all transmitted pilot patterns are the same, they will interfere with each other in the user equipment (UE), which in turn degrades system throughput and the quality of channel estimation.

In [28], Costas array-based pilot patterns are investigated. Authors in [28] show that Costas array-based two-dimensional pilot pattern has minimal collisions with its arbitrary time shifted versions. In their later work [29], both link and system level performances of Costas array-based pilot patterns are evaluated. However, the number of unique pilot patterns that are generated via Costas array is still limited, especially when the system is not synchronized in time. Latin square-based pilot pattern design is proposed and investigated in [30] and [31]. However, wide variations in system performance (e.g., BER) are observed in Latin square-based method, which highly limits its application.

1.4 Motivation and Contributions

1.4.1 Motivation

Surveying the prior works in the literature, we find that limited research efforts have focused on coping with the inherent disadvantages regarding OFDM in cellular OFDMA systems. Since PAPR reduction techniques in single user OFDM can be easily extended to downlink OFDMA, in this work, we mainly concentrate on (a) FH pattern design for minimizing/averaging intra/inter-cell interference, (b) pilot pattern design for improving the quality of channel estimation, and (c) pilot pattern design for facilitating time-frequency

synchronization and device identification in multi-cell OFDMA.

Regarding (a), desired FH patterns should minimize intra-cell interference to zero (i.e., orthogonal within a cell), and well average inter-cell interference. However, existing FH pattern design methods (e.g., Latin-square and Costas-array based approaches) either result in variations in system performance (such as BER), or lack of abilities to exploit frequency diversity gains. Therefore, investigating novel methodology to design FH patterns that avoid disadvantages of existing schemes becomes crucial.

For the second aspect, in a multi-cell multi-antenna environment, typical comb-type or block-type based pilot pattern designs are not suited any more. This is because their structured/periodic nature significantly increases the probability of pilot-to-pilot collisions among adjacent cells. From the standpoint of system level, high probability of pilot-to-pilot collisions degrades entire system throughput. Therefore, there is a need for pilot pattern design such that, (1) the full channel response can be interpolated with a limited number of two-dimensional pilot signals. That is, in the context of OFDM, in order to fulfill Nyquist sampling theorem, there exist both a minimum subcarrier spacing and a minimum symbol spacing between pilots; (2) the number of different pilot patterns should be as large as possible with each pair of the pilot patterns having a small maximum number of collisions.

With respect to (c), finding predefined pilot patterns that have good correlation properties, or ambiguity function, can facilitate system time-frequency synchronization and device identification. It has been known that some specific integer sequences, such as linear congruences, exhibit good auto-correlation property and ambiguity function. Hence, if (b) is taken into account as well, it is our objective to design proper pilot patterns such that (i) channel estimation task can be performed efficiently and effectively, (ii) time-frequency offsets can be correctly recovered, and (iii) devices/users can be easily identified in a multi-cell environment.

1.4.2 Contributions

This section describes the key contributions of this thesis:

1. *We propose and evaluate the use of residue number system (RNS) arithmetic in designing orthogonal FH patterns, that are especially suited for downlink OFDMA.*

   In this thesis, we first show that different RNS sequences exhibit orthogonality to each other by contradiction. Then, according to finite field theory, we obtain the number of symbol-to-symbol collisions between different RNS-based FH patterns. Using these results, we construct FH patterns that minimize the intra-cell interference to zero, and average the inter-cell interference. Comparing to existing methods, RNS-based approach shows consistent system performance among all cells, and provides more frequency diversity gains. These results have been presented in our peer reviewed articles [32][33].

2. *We propose and evaluate the use of RNS arithmetic in constructing two-dimensional pilot patterns, that are suited for multi-cell multi-antenna downlink OFDMA.*

   By giving integer addresses to pilot signals, their positions in both time and frequency can be determined via RNS arithmetic such that: (1) channel's time-frequency response can be sampled at Nyquist rates; and (2) a large number of unique pilot patterns are assigned to adjacent cells. From the standpoint of link level, our proposed approach shows the same error rate performance as conventional two-dimensional pilot pattern design. From a system level perspective, RNS-based pilot pattern design significantly enhances system throughput as compared to existing schemes. This aspect has been covered in [34].

1.5 Organization

The rest of this thesis is organized as follows. Chapter 2 introduces residue number system arithmetic in detail. By comparing RNS with conventional number system (CNS), we conclude that RNS arithmetic has good properties that benefit both computer hardware implementation and communication. In Chapter 3, detailed procedures of constructing RNS-based FH patterns are presented. In Chapter 4, RNS-based pilot pattern design is introduced along with experimental results showing that the proposed approach shows superior performance from both link level and system level perspectives. Finally, we present the conclusions of this thesis and suggest possible future research directions.

Chapter 2

Residue Number System Arithmetic

The main objective of this chapter is to introduce residue number system (RNS) arithmetic. Then, after briefly reviewing applications of RNS in communication systems, we highlight its properties that are most related to FH/pilot pattern design in downlink OFDM/OFDMA. Before introducing RNS, we start by giving an overview of conventional number system (CNS) from a computer arithmetic's point of view.

2.1 Conventional Number System

In general, numbers may be signed. For binary representations of these signed numbers, there are three standard notations that are widely used. These are *sign-and-amplitude*, *one's complement* and *two's complement* [35].

The *sign-and-magnitude* notation is quite simple and common. It is derived from the conventional written notation of representing a negative number by assigning a sign to a magnitude that represents a positive number [36]. In computer computations, the higher-order bit of an binary input is usually used as the sign bit. That is, a sign bit of 0 represents a positive number, while a sign bit of 1 indicates a negative number. However, addition and substraction are much harder to implement by using *sign-and-magnitude* notation, which highly limits its application in the context of binary computer hardware.

In *one's complement* notation, the representation of the negation of a number is obtained by inverting the bits in its binary representation; that is, the 0s are changed to 1s and the 1s are changed to 0s [36]. Although *one's complement* notation is more efficient than *sign-and-magnitude* notation regarding computer arithmetic, it is still harder to implement than *two's complement* notation, especially when multiplication and division are taken into account.

The *two's complement* notation is the most popularly used computer arithmetic among the three. This can be clearly revealed by its operation. Negation in *two's complement* notation consists of a bit-inversion followed by the addition of a 1, with any carry from the addition being ignored. From above descriptions, we can see that algorithm and hardware designs required for its implementation are straightforward, and computer arithmetic operations are significantly simplified.

2.2 Residue Number System

Residue number system (RNS) is an integer number system, which is developed based upon Chinese Remainder Theorem (CRT) appeared in a book by Sun Tze 100 A.D. [37]. Comparing with conventional number system, RNS is more complex to implement from a computer hardware's point of view. However, in 1950s, with the rapid evolution of digital computer and microelectronics technology, RNS became an attractive computer arithmetic in computer architecture. Pioneer works in RNS computational hardware can be found in [38][39][40]. In addition, RNS has two inherent features that are attractive relative to CNS. They are: (1) the carry-free arithmetic and (2) the lack of ordered significance among the residue digits [41]. The first property implies that errors that are generated during arithmetic operations do not propagate due to the absence of a carry forward, and therefore, do not corrupt other residue digits. The second property indicates that discarding redundant residue digits will not affect the final result. This property invokes the use of redundant residue number system (RRNS) in digital processors for self-checking, error-detection and correction. In recent years, many research efforts have been put into this area, including

Integer N_k	Moduli	Residues
$N_1 = 3$	{2,3,5}	{1,0,2}
$N_2 = 36$	{4,5,7}	{0,1,1}
$N_3 = 100$	{7,8,9}	{2,4,1}

Table 2.1: *RNS representation of the integer* N_k

[42] and [43] as representative examples. A more comprehensive overview of applications of RRNS in modern digital communication systems (e.g., DS-CDMA) can be addressed to [44].

2.2.1 Residue Number System Transform and Its Inverse

Residue number system is defined by the choice of v number of positive integers m_i ($i = 1, 2, \cdots, v$), referred to as moduli [41]. If all the moduli are pairwise relative primes to each other, any integer N_k which falls in the range of $[0, M_r)$ can be uniquely and unambiguously represented by the residue sequence $(r_{k,1}, r_{k,2}, \cdots, r_{k,v})$, where $M_r = \prod_{i=1}^{v} m_i$ and $r_{k,i} = N_k \text{mod}\{m_i\}$ for $i = 1, 2, \cdots, v$. $[0, M_r)$ is defined as the dynamic range of the RNS. Mathematically, above descriptions can be expressed as

$$N_k \Longleftrightarrow (r_{k,1}, r_{k,2}, \cdots, r_{k,v}), \tag{2.1}$$

$$r_{k,i} = N_k \text{mod}\{m_i\}, i = 1, 2, \cdots, v. \tag{2.2}$$

Illustrative examples of RNS representations of integer messages are given in Table 2.1. From Table 2.1, it is easy to conclude that any integer in the dynamic range of RNS, can be unambiguously represented by the corresponding residues.

The inverse transform of the conventional weighted number system (integer number system here) to RNS domain is straightforward to finalize thanks to the so-called Chinese Remainder Theorem (CRT) [45][46]. CRT is well known for its capability of solving a set of linear congruences simultaneously. According to CRT, it can be shown that by given any

v-tuple $(r_{k,1}, r_{k,2}, \cdots, r_{k,v})$, where $0 \leq r_{k,i} < m_i$ for $i = 1, 2, \cdots, v$, there exists one and only one integer N_k such that $r_{k,i} = N_k \text{mod}\{m_i\}$ and most importantly, $0 \leq N_k < M_r$. Mathematically, the numerical value of N_k can be computed as [47]:

$$N_k = \sum_{i=1}^{v} r_{k,i} a_i M_i \text{mod} M_r, \tag{2.3}$$

where, $M_i = \frac{M_r}{m_i}$ and $a_i = M_i^{-1} \text{mod}\{m_i\}$ for $i = 1, 2, \cdots, v$.

2.2.2 Properties of Residue Number System

In this subsection, properties of RNS that are most relevant to FH/pilot pattern design in downlink OFDMA are investigated.

We start by showing basic arithmetic operations of RNS. Assuming that integers N_1 and N_2 have residues (RNS representations) of $N_1 \Longleftrightarrow (r_{1,1}, r_{1,2}, \cdots, r_{1,v})$ and $N_2 \Longleftrightarrow (r_{2,1}, r_{2,2}, \cdots, r_{2,v})$, respectively.

Property 1: The arithmetic operations over the RNS domain can be expressed as [48]

$$N_1 \bullet N_2 \Longleftrightarrow [(r_{1,i} \bullet r_{2,i})(\text{mod} m_i)]_{i=1}^{v}, \tag{2.4}$$

where, $\bullet$ *represents ordinary addition, substraction, or multiplication of two integers (on the left hand side), or on the basis of the residue digits with respect to their corresponding modulus (on the right hand side).* □

This property implies that, one can convert conventional binary arithmetic operations involving large integers to residue arithmetic operations, carried out by small residues. Since these arithmetic operations are executed in parallel, there will be no carry forward between residue digits, which prevents the error propagation among the residues [44]. In addition, property 1 can be easily extended to the case where arithmetic operations of multiple integers (more than two) are taken into account.

Property 2: RNS representations (residue digits) of different integer messages within the same dynamic range, are unique. □

Proof: we need to show that every N_k in the range of $[0, M_r)$, has a unique residue set that is different from residue sets generated by other integers within the same dynamic range. We will prove this by contradiction as follows:

Assuming N_1 and N_2 are different integers which are in the same range of [0, M_r) with the same residue set. That is,

$$N_1 \text{mod}\{m_i\} = N_2 \text{mod}\{m_i\}, i = 1, 2, \cdots, v. \tag{2.5}$$

Therefore, we have

$$(N_1 - N_2) \text{mod}\{m_i\} = 0. \tag{2.6}$$

Thus, we can conclude from (2.6) that $N_1 - N_2$ is actually the least common multiple (LCM) of m_i. Furthermore, if m_i are pairwise relative primes to each other, their LCM is $M_r = \prod_{i=1}^{v} m_i$ and it must be that $N_1 - N_2$ is a multiple of M_r. However, this statement does not hold since $N_1 < M_r$ and $N_2 < M_r$. Therefore, by contradiction, N_1 and N_2 should not have the same residue set. ■

Property 2 is also known as "orthogonality" property of RNS sequences, and is very important to FH sequence/pattern design in multiple access (MA) systems. We will discuss this aspect in detail in the following Chapter 3.

Property 3: The maximal number of collisions between any two RNS sequences under arbitrary mutual non-zero periodic time shift is one. □

Proof: In order to characterize the maximal number of collisions between each pair of the RNS sequences, we first look into the general solution that is derived based upon finite field theory, which includes RNS sequence as a special case.

An integer sequence can be defined as a set of G frequencies from a finite set of Q frequencies. If Q is a prime, an one-to-one representation between the set of Q frequencies and the Galois filed of Q elements (i.e., GF(Q)) can be obtained. In other words, the integer sequence of length G $(f_i, i = 0, 1, \cdots, G-1)$ can be generated by the corresponding associated polynomials of at most degree d, which is a set of elements in GF(Q) [31].

Equivalently, the integer sequence can be expressed as

$$f_i = P(i), i = 0, 1, \cdots, G-1, \tag{2.7}$$

$$P(x) = \sum_{j=0}^{d} n(j)x^j, \tag{2.8}$$

where, Q is a prime, and coefficient $n(d-1)$ is fixed for all associated polynomials, all other $n(j)$ can be chosen as all possible values in GF(Q) [49].

In general, the number of collisions between two different sequences is defined as the cross-correlation of these two sequences. Assume p and r as two different integer sequences and their associated polynomials are $P(x)$ and $R(x)$, respectively. Then, the difference between these two polynomials can be calculated as

$$E(x) = P(x) - R(x) = \sum_{j=0}^{d} e(j)x^j. \tag{2.9}$$

From (2.9), we can see that $E(x)$ is at most of degree d. This indicates that sequences p and r are identical to each other at most d positions (and therefore, resulting in at most d roots of $E(x)$). From the cross-correlation's point of view, (2.9) implies that the cross-correlation of two different integer sequences is no more than d, which is equivalent to say that the maximal number of collisions between such two sequences is no more than d. For $d = 1$, the set of linear congruence sequences is obtained, which includes RNS sequences as a special case [41]. ■

It is also worth noting here that, property 3 is critical in predetermined pilot pattern design, as it reveals that RNS can provide more degrees of freedom for generating unique pilot patterns that do not interfere with each other at the user's equipment (UE). Detailed descriptions and analysis are given in following chapters.

2.3 Summary

In this chapter, we briefly discuss the residue number system arithmetic associated with its properties. Following the RNS arithmetic, look-up tables containing both integer messages

and residue digits can be built in advance. This off-line process facilitates the arithmetic operations at UEs, where computational complexity is a critical budget. With the knowledge of residues and modulus, CRT is used to recover the integers. Important properties of RNS regarding practical concerns are provided. With these properties, designing orthogonal FH patterns, or constructing collision-free pilot patterns in downlink OFDMA becomes possible.

Chapter 3

RNS aided FH Pattern Design in Downlink OFDMA

In this chapter, RNS aided FH pattern design in downlink OFDMA is introduced in detail. We start by giving the system model of conventional FH-OFDMA, then analytically show the symbol collision probabilities underlying this conventional hopping scheme. After that, our proposed RNS-based FH pattern design method is given associated with illustrative examples. In this part, property 2 of RNS sequences (as shown in chapter 2) play an important role that guarantees zero collisions among constructed FH patterns within the same cell. By comparing with previous works, advantages of our proposed approach can be clearly revealed. Finally, corresponding numerical results are provided to verify the effectiveness of RNS-based method, which show that, indeed the new paradigm outperforms the existing schemes in many aspects.

3.1 System Model of Coded Frequency-Hopped OFDMA

In this section, we first describe the signal transmission scheme for each individual user in an OFDMA system. Then, we introduce the access model and interference model under both independent and cluster hopping schemes.

3.1.1 Signal Transmission Scheme

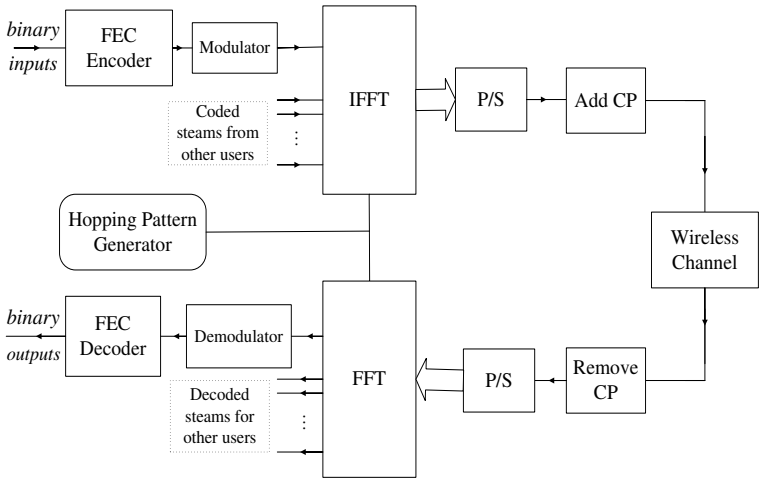

Figure 3.1: *The block diagram of coded FH-OFDMA system.*

The block diagram of FEC (Forward Error Correction) coded FH-OFDMA system is shown in Fig.3.1. Here, data bits of every user are first channel coded and then mapped to complex constellation points. We assume that there are M users in the system, utilizing a total of N OFDM subcarriers. Each user is assigned a specific set of subcarriers out of the total available subcarriers according to his/her data rates. Let N_i be the number of subcarriers allocated to user i. Then, user i transmits the information symbols $\mathbf{x}^i = (x_1^i, x_2^i, \cdots, x_{N_i}^i)^T$ ($(\cdot)^T$ represents the transpose operation) on the assigned N_i subcarriers. Therefore, the baseband transmitted signal of user i can be expressed as,

$$s^i(t) = \sum_{k=1}^{N_i} x_k^i e^{j2\pi \frac{k}{T} t}, 0 \leq t < T, \tag{3.1}$$

where, $s^i(t)$ represents the time domain signal and T denotes one OFDM symbol duration. Since this is an OFDMA system, it is important to remember that every user is assigned a different set of subcarriers for transmission and this allocation is dynamic in the case of frequency hopping OFDMA. That is, in the IFFT module, the frequency assignment follows a predetermined FH pattern. Moreover, each user transmits zeros on subcarriers which are

not assigned to him/her.

For convenience, we note C_i as the subcarrier set that is assigned to user i. Hence, $N \times 1$ information symbols vector of user i can be written as

$$\mathbf{x}^i(k) = \begin{cases} 0, k \notin C_i \\ x_k^i, k \in C_i \end{cases} . \tag{3.2}$$

The discrete form of the transmitted signal $s^i(t)$ is then given as,

$$\mathbf{s}^i = \mathbf{F}\mathbf{x}^i, \tag{3.3}$$

where $\mathbf{F}$ is the IFFT matrix defined as

$$\mathbf{F} = \frac{1}{\sqrt{N}} \begin{pmatrix} W_N^{00} & \cdots & W_N^{0(N-1)} \\ \vdots & \ddots & \vdots \\ W_N^{(N-1)0} & \cdots & W_N^{(N-1)(N-1)} \end{pmatrix} \tag{3.4}$$

where $W_N^{pq} = e^{j2\pi pq/N}$.

Let $\mathbf{h}^i = [h^i(0), h^i(1), \cdots, h^i(N-1)]$ denote the channel impulse response vector, then its Fourier transform is

$$\mathbf{H}^i = \mathbf{F}^H \mathbf{h}^i, \tag{3.5}$$

where $(\cdot)^H$ represents the Hermitian transpose. In general, each channel impulse response is a function of time and access delay which can be modeled as a tapped delay line, i.e.,

$$h^i(\tau, t) = \sum_{l=1}^{L} h_l^i(t)\delta(\tau, \tau_l), \tag{3.6}$$

where L is the number of multi-paths and τ_l is the time delay of the *l-th* path. The tap coefficients are independent, zero-mean, circularly symmetric complex Gaussian random processes at each instant t, i.e., $h_l^i(t) \sim CN(0, \sigma_l^2)$ with the total power normalized to unity, i.e., $\sum_{l=1}^{L} \sigma_l^2 = 1$. In this work, we use Jakes' model to describe the time/frequency variation of each channel coefficient. Therefore, the spaced frequency ($\triangle f$) spaced time ($\triangle t$) correlation function of the channel frequency response can be expressed as [50]

$$r_H(\triangle f, \triangle t) = \sum_{l=1}^{L} \sigma_l^2 J_o(2\pi f_D \triangle t) e^{-j2\pi \triangle f \tau_k}, \tag{3.7}$$

where, f_D is the Doppler frequency.

At the receiver end, after FFT, the received signal corresponding to user i on subcarrier k is

$$\mathbf{r}^i(k) = \mathbf{H}^i(k)\mathbf{x}^i(k). \tag{3.8}$$

Then, the overall received signal which is a superposition of the signals transmitted from all M users is

$$\begin{aligned} \mathbf{r}(k) &= \sum_{i=1}^{M} \mathbf{r}^i(k) + \mathbf{n}(k) \\ &= \sum_{i=1}^{M} \mathbf{H}^i(k)\mathbf{x}^i(k) + \mathbf{n}(k), \end{aligned} \tag{3.9}$$

where $\mathbf{n}(k)$ is the Fourier transform of the noise vector.

3.1.2 Access Model

In this part, clustered and independent FH-OFDMA are introduced and closed form expressions of the expected number of collisions per symbol under both of these two hopping strategies are presented.

Clustered FH-OFDMA

In cluster hopping, each user selects a set of continuous subcarriers, termed as cluster, to transmit the information symbols. Specifically, the hopping takes place among clusters of subcarriers based on predetermined FH patterns. Therefore, collisions occur among clusters first, and then across all OFDM subcarriers within that cluster. The expected number of symbol losses per cluster collision corresponds to [21]

$$E_c = N_c P_{int}, \tag{3.10}$$

where, N_c is the number of subcarriers per cluster and P_{int} represents the probability that at least one interfering user collides with the desired user. For cluster hopping, we have

N/N_c hopping clusters. Therefore, the collision probability between the desired user and the interfering user in one cluster is $1/(N/N_c)$. Hence, the probability that at least one of the $M-1$ users collide with the desired user can be expressed as

$$P_{int} = 1 - \left(1 - \frac{1}{N/N_c}\right)^{M-1}. \tag{3.11}$$

For convenience, throughout the rest of this chapter, we assume that each user employs the same number of subcarriers (N_c) per cluster.

Independent FH-OFDMA

In independent hopping, subcarriers occupied by a user are selected independently from all available subcarriers. In other words, N_c subcarriers in one cluster are not continuous anymore and they are chosen in a pseudo-random fashion across the frequency spectrum. With independent hopping, the expected number of symbols lost per symbol collision is given by [21]

$$E_{\tilde{c}} = \sum_{x=1}^{N_c} x p_{N_c}(x), \tag{3.12}$$

where $p_{N_c}(x)$ is the probability that x subcarriers out of N_c subcarriers occupied by each user experience collisions due to interfering users.

Theorem 3.1.1. *For independent FH-OFDMA scheme described above, $p_{N_c}(x)$ corresponds to*

$$\begin{aligned} p_{N_c}(x) &= \binom{N_c}{x} \left[1 - \left(\frac{N - 2N_c + x}{N - N_c + x}\right)^{M-1}\right]^x \\ &\times \left(\prod_{y=0}^{N_c-1} \frac{N - N_c + x - y}{N - y}\right)^{M-1}. \end{aligned} \tag{3.13}$$

Proof: $p_{N_c}(x)$ is the probability that x subcarriers of the desired user collide with the subcarriers of interfering user given that each user occupies a total of N_c subcarriers. It is evident that the number of possible combinations of x subcarriers that experience collisions

is $\begin{pmatrix} N_c \\ x \end{pmatrix}$. Define $q_{N_c}(a)$ as the probability that a symbols are collision-free given that each user occupies N_c subcarriers. Furthermore, define $p_{N_c}(b|c)$ as the conditional probability that b symbols collide given that c symbols are collision-free. Therefore, we can write $p_{N_c}(x)$ as

$$p_{N_c}(x) = \begin{pmatrix} N_c \\ x \end{pmatrix} q_{N_c}(N_c - x) p_{N_c}(x|N_c - x). \tag{3.14}$$

Here, $q_{N_c}(N_c - x)$ corresponds to

$$q_{N_c}(N_c - x) = \left(\prod_{k=0}^{N_c-1} \frac{N - (N_c - x) - k}{N - k} \right)^{M-1}. \tag{3.15}$$

(3.15) denotes the probability that the desired user's remaining $N_c - x$ subcarriers are collision-free while none of the other $M - 1$ users within the same cell occupies these subcarriers. $p_{N_c}(x|N_c - x)$ is expressed as [21]

$$p_{N_c}(x|N_c - x) = \left[1 - \left(\frac{N - 2N_c + x}{N - N_c + x} \right)^{M-1} \right]^x. \tag{3.16}$$

(3.16) represents the conditional probability that each of the x subcarriers of the desired user collide given that the other $N_c - x$ subcarriers are collision-free. By substituting (3.15) and (3.16) into (3.14), we obtain the result in (3.13). ■

3.1.3 Interference Model

In this paper, we model inter-cell interferences as additive complex Gaussian distributed distortions. This model is accurate when interferences from adjacent cells are perfectly randomized with respect to the cell of interest. Models specific to clustered and independent FH-OFDMA are presented in the following.

Clustered FH-OFDMA

In clustered FH-OFDMA, if interference occurs on any symbol on one subcarrier in the cluster, all other symbols in the same cluster will also experience interferences from adjacent

cells. Hence, the interference for the i-th user can be modeled as,

$$\mathbf{r}^i = \mathbf{H}^i\mathbf{x}^i + \mathbf{n}^i + \mathbf{e}^i, \tag{3.17}$$

where $\mathbf{r}^i$ is a $N_c \times 1$ vector, representing the received signal of user i; $\mathbf{x}^i$ is the $N_c \times 1$ transmitted signal vector; $\mathbf{H}^i$ is a $N_c \times N_c$ matrix that contains the frequency domain representations of channel impulse response; $\mathbf{n}^i$ is a $N_c \times 1$ vector whose components are complex Gaussian random variables with zero mean, and variance σ^2. Here, the $N_c \times 1$ vector $\mathbf{e}^i$ is the interference vector that captures the interference from all adjacent cells. The components of $\mathbf{e}^i$ are i.i.d complex Gaussian random variables independent of $\mathbf{x}^i$, $\mathbf{H}^i$ and $\mathbf{n}^i$ with mean zero, variances $(\widetilde{\sigma}_1^2, \cdots, \widetilde{\sigma}_{N_c}^2)^T$. The variances correspond to,

$$\widetilde{\sigma}_j^2 = \rho E_s/SIR_s, j = 1, 2, \cdots, N_c, \tag{3.18}$$

where SIR_s denotes the symbol signal-to-interference ratio and $\rho \in \{1, 0\}$ characterizes the presence/absence of a collision between users in different cells. That is, if there is a collision, ρ equals to one and if there is no collision, ρ is set to zero. Furthermore, ρ can be modeled as a bernoulli random variable with probability of collision equals to p (i.e., $P(\rho = 1) = p$ and $P(\rho = 0) = 1 - p$), which can be expressed as

$$p = 1 - (1 - \frac{1}{N/N_c})^{M-1}, \tag{3.19}$$

where, M is the number of active users. If the system is fully loaded, then $M = N/N_c$. If there is a collision, i.e., $\rho = 1$, then all subcarriers in the cluster will be affected by the inter-cell interference.

Independent FH-OFDMA

In independent hopping, since subcarriers are selected independently of all other subcarriers according to predetermined FH patterns, collisions occur independently. Hence, for the k-th subcarrier of the i-th user,

$$\mathbf{r}^i(k) = \mathbf{H}^i(k)\mathbf{x}^i(k) + \mathbf{n}^i(k) + \mathbf{e}^i(k). \tag{3.20}$$

Here, the interference power $\widetilde{\sigma}^2$ of the i.i.d complex Gaussian random variable $\mathbf{e}^i(k)$ corresponds to,

$$\widetilde{\sigma}^2 = \rho E_s / SIR_s, \tag{3.21}$$

where $\rho = 1, 0$ with probabilities p and $1 - p$, respectively. The collision probability p is given by,

$$p = 1 - (1 - \frac{1}{N})^{MN_c - 1}. \tag{3.22}$$

For a fully loaded system with independent hopping, M is identical to N, N_c becomes to one.

3.2 RNS-FH Pattern Design

The determination of FH patterns better satisfies the following conditions [19]: (i) minimize intra-cell interference; (ii) average inter-cell interference; (iii) avoid ambiguity while identifying users, and (iv) exploit frequency diversity by forcing hops to span a large bandwidth. The first aspect is relatively easy to achieve by using orthogonal hopping patterns within a cell. To average inter-cell interferences, hopping patterns are constructed in a way that two users in different cells interfere with each other only during a small fraction of all hops. The third condition requires base stations to have the capability of distinguishing different users efficiently according to their unique FH signatures. Finally, the last requirement not only ensures the security of the transmission, but also mitigates the effect of fading by exploiting frequency diversity.

Following the RNS arithmetic, we propose to design FH patterns that satisfy all the requirements described above. Detailed procedures of constructing RNS-FH patterns are given in the following two parts. The first part describes the two-stage algorithm, while the second part introduces the multi-stage algorithm which can be considered as generalization of the two-stage algorithm.

Two-stage Algorithm

In this part, the detailed procedures of constructing RNS-FH patterns via a so-called two-stage algorithm is introduced. We present the algorithm for a cluster hopping OFDMA system. It is straightforward to extend the algorithm to the independent hopping scenario. The steps involved in the two-stage selection algorithm are given as follows:

1. Divide the total available subcarriers N into M_c clusters with each cluster containing N_c number of contiguous subcarriers.

2. If M_c can be written as a product of two pairwise relative primes, e.g., $M_c = a_1 \cdot b_1$, we can first group M_c clusters into a_1 groups with b_1 clusters in each group. Then, we index the groups from 0 to $a_1 - 1$.

3. Index the clusters in each group from 0 to $b_1 - 1$.

4. At the 0-th time slot, assign integer N_k to user k as its FH address according to its access order to the system, where $0 < N_k \leq M_c$.

5. If $N_k \text{mod}\{a_1, b_1\} = \{\hat{a}_1, \hat{b}_1\}$, then user k selects the $\hat{b}_1$-th cluster out of the $\hat{a}_1$-th group for transmission.

6. At the t_s-th time slot, assign integer $N_k + t_s$ to user k as its current FH address and repeat step 5.

7. Repeat steps 4 - 6 until one mutually orthogonal FH pattern is obtained.

8. If M_c can be expressed as products of other combinations of two pairwise relative primes, e.g., $M_c = a_2 \cdot b_2 = \cdots = a_w \cdot b_w$, then w different orthogonal FH patterns can be obtained by repeating steps 2 - 7, w times.

An example is given in Fig.3.2 to illustrate the two-stage RNS assisted frequency hopping strategy. Here, 6 users access the system ($M = 6$); the total number of subcarriers is 30

($N = 30$) and they are divided into 6 clusters ($M_c = 6$) with each cluster containing 5 contiguous subcarriers ($N_c = 5$). At the 0-th time slot, the FH address assigned to the 5-th user is 5 according to his/her access order to the system. Therefore, 5 mod $\{2, 3\} = \{1, 2\}$. User 5 will choose the 2-nd cluster of subcarriers out of the 1-st group of clusters to transmit. At the 1-st time slot, the FH address assigned to this user becomes $5 + 1 = 6$. Obviously, 6 mod $\{2, 3\} = \{0, 0\}$, then he/she will select the 0-th cluster of subcarriers out of the 0-th group of clusters for transmission at this time. This process continues until one FH sequence of length M_c is constructed.

Multi-stage Algorithm

The multi-stage algorithm is an extension of the two-stage algorithm. Introducing the multi-stage algorithm can not only enhance the flexibility of the pattern design, but also strengthen the robustness of the entire FH scheme. We describe the multi-stage algorithm assuming an independent hopping scheme with each user employing the same number of subcarriers, i.e., $N_i = N_c$, for $i = 1, 2, \cdots, M$. The steps involved in the multi-stage algorithm correspond to:

1. If N can be written as a product of m pairwise relative primes, e.g., $N = a_1 \cdot b_1 \cdot c_1 \cdots$, we can first group N subcarriers into a_1 groups with b_1 sub-groups in each group. Then, we index the first-stage groups from 0 to $a_1 - 1$.

2. Index the second-stage groups in each first-stage group from 0 to $b_1 - 1$. Then group the subcarriers in each second-stage group into c_1 sub-groups.

3. Similar steps continue on until all of the subcarriers are grouped and indexed at the mth-stage.

4. At the 0-th time slot, assign integer set $\{N_k, N_k+M, \cdots, N_k + MN_c\}$ to user k as its FH addresses, where N_k is its access order to the system, $0 < N_k \leq N$.

5. If $N_k \text{mod}\{a_1, b_1, c_1, \cdots\} = \{\hat{a}_1, \hat{b}_1, \hat{c}_1, \cdots\}$, then user k first selects the $\hat{b}_1$-th second-stage group out of the $\hat{a}_1$-th first-stage group, then similar selecting procedures continue on until the subcarrier at the mth-stage has been extracted out for transmission.

6. The process in step 5 is repeated on the other elements in the integer set of user k until N_c subcarriers have been extracted out for user k to transmit.

7. At the t_s-th time slot, assign integer set $\{N_k + t_s, N_k + M + t_s, \cdots, N_k + MN_c + t_s\}$ as the current FH addresses of user k and repeat steps 5 - 6.

8. Repeat steps 4 - 7 until one mutually orthogonal FH pattern is obtained.

9. If N can be expressed as products of other combinations of m pairwise relative primes, e.g., $N = a_2 \cdot b_2 \cdot c_2 \cdot \cdots = \cdots = a_w \cdot b_w \cdot c_w \cdot \cdots$, then w different orthogonal FH patterns can be obtained by repeating steps 1 - 8, w times.

It is easy to visualize the multi-stage algorithm by using a tree-diagram. An example is given in Fig.3.3. Here, 30 users access the system ($M = 30$); a total of 30 subcarriers are used, i.e., $N = a_1 \cdot b_1 \cdot c_1 = 2 \cdot 3 \cdot 5 = 30$. Two specific examples are illustrated as follows: (1) Consider user 2. The subcarriers used by this user at the 0-th time slot can be calculated as follows: $2 \text{ mod } \{2, 3, 5\} = \{0, 2, 2\}$; i.e., in the 0-$th$ first-stage group, the 2-nd subcarrier out of the 2-nd second-stage group is selected for transmission. This is indicated with a solid line in Fig.3.3; (2) Consider user 27. $27 \text{ mod } \{2, 3, 5\} = \{1, 0, 2\}$; i.e., in the 1-$st$ first-stage group, the 2-nd subcarrier out of the 0-th second-stage group is selected by the 27-th user for transmission at the 0-th time slot. This is indicated with a dashed line in the figure. This procedure continues until an FH sequence of length N is completed. We should note that, in this example, the system is fully loaded ($M = N = 30$). For $M < N$, each user is assigned a set of FH addresses rather than one unique FH signature. For example, consider user 2 in Fig.3.3, the 2-nd subcarrier occupied by user 2 at the 0-th time slot is determined starting from his/her current FH address $2 + 30 = 32$ and following the steps as before.

These steps are repeated until N_c subcarriers for user 2 are identified. Extrapolating the procedure across the time axis, an entire FH sequence of length N is designed.

With respect to the design procedures, the major difference between independent hopping and cluster hopping is the following: in independent hopping, each FH address specifies a single subcarrier that can be used. Therefore, if users have very high bandwidth/rate or other QoS requirements, multiple FH addresses can be given to accommodate. In cluster hopping scenario, a user may demand only one unique FH address as a single address completely specifies all N_c subcarriers required for transmission. Fully loaded independent hopping system is a special case of cluster hopping with one subcarrier in each cluster.

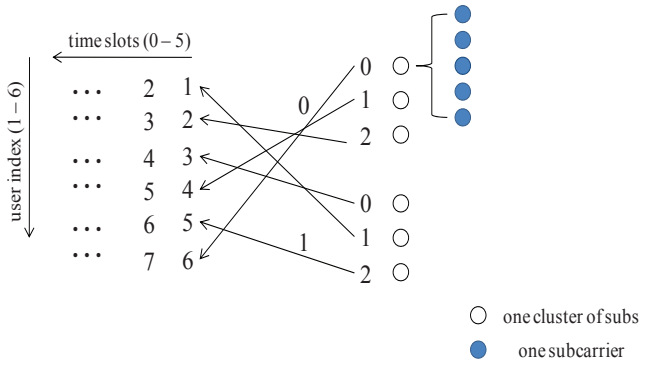

Figure 3.2: *One example of RNS assisted two-stage hopping strategy.*

From Fig.3.2 and 3.3, it is evident that the proposed RNS-FH patterns guarantee the orthogonality among different users within a cell. That is, users within the same cell will not interfere with each other when they simultaneously access the system. The next example, which is shown in Fig.3.4, demonstrates that if different RNS-FH patterns are assigned to adjacent cells, inter-cell interferences can be perfectly averaged. In this example, N is set to 10 while the moduli sets used to construct FH patterns in cell 1 and 2 are $\{a_1 = 2, b_1 = 5\}$ and $\{a_2 = 5, b_2 = 2\}$, respectively. From Fig.3.4, it is evident that every user in cell 1 experiences interference from different users from cell 2 during each of his/her hops. For example, in the first OFDM symbol duration, user 1 in cell 1 is interfered by user 8 from

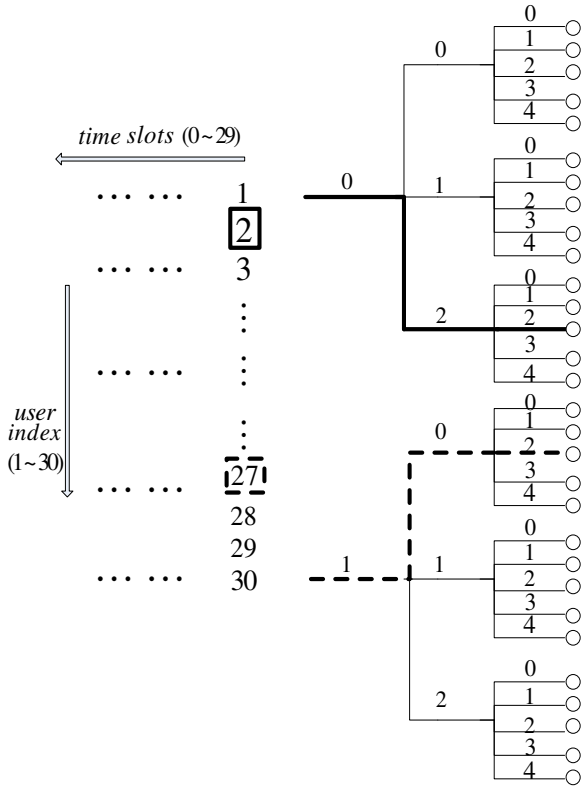

Figure 3.3: *One example of RNS assisted multi-stage hopping strategy.*

cell 2; in the next OFDM symbol slot, user 1 is interfered by user 5 from cell 2 and so on. In general, users from different cells collide only once during a frequency hopping cycle under the proposed scheme. Therefore, full interference diversity is exploited in the case of RNS-FH patterns.

The properties of the proposed RNS-FH patterns can be summarized below:

1. At most, a size of $N \times N$ mutually orthogonal FH pattern can be obtained for the independent hopping scheme. The size becomes $M_c \times M_c$ for the cluster hopping.

2. If N (M_c) can be written as a product of m pairwise relative primes, then at least, $(m-1)m!$ different RNS-FH patterns can be obtained.

3. With the use of the same moduli set, for independent hopping, RNS-FH patterns

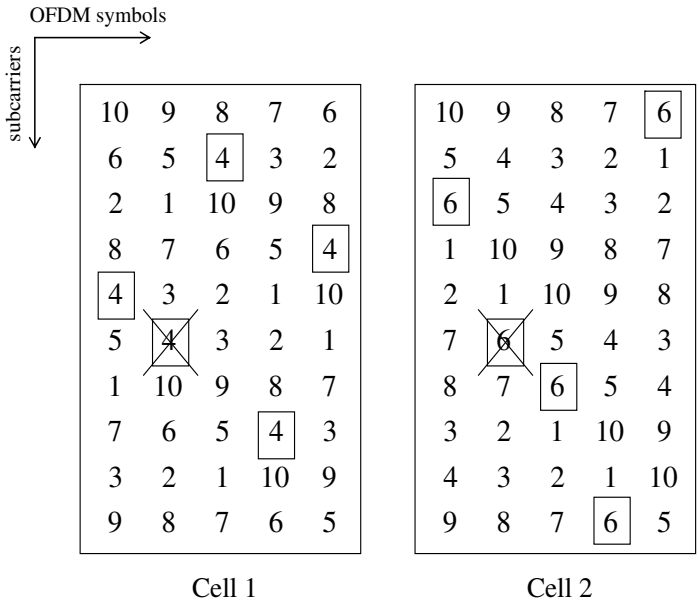

Figure 3.4: *Two different FH patterns are given and their only collision point is highlighted.*

constructed after N frames (M_c for cluster hopping) are actually periodical extensions of the RNS-FH pattern designed during the first $N(M_c)$ frames.

4. With knowledge of moduli and residue, the base station can regenerate the entire RNS-FH pattern using the CRT.

3.3 Simulation Results

Parameters of the simulated system are provided in Table 3.1. The cyclic prefix within one OFDM symbol duration is assumed long enough to eliminate ISI (inter-symbol interference). Two 6-ray channel pulse responses are considered following the UTRA Vehicular Test Environment [51]. In Fig.3.5, the correlation functions of these two channels are plotted versus the variation of Δf, while $\Delta t = 1$ slot and $f_D T_s = 0.01$. From Fig.3.5 we can conclude that if small hopping intervals occur frequently in a FH pattern, Veh B can provide more

Table 3.1: *System Parameters of frequency hopped OFDMA*

Transmission BW	5MHz
Carrier frequency	2GHz
OFDM symbol duration	$100\mu s$
CP duration	$10\mu s$
Tone spacing	11KHz
FFT size	128
Occupied Subcarriers	110
Channel impulse response	Veh A / Veh B
Channel coding	1/2 convolutional code
Modulation	QPSK
Time slots	10

frequency diversity than Veh A.

Theoretical (see equations (3.10) and (3.12)) and simulated expected number of collisions per symbol in RNS-FH OFDMA are given in Fig.3.6. The high collision probability severely limits the number of active users that can be simultaneously supported by the FH system.

In Fig.3.7, bit error rate (BER) versus SNR of RNS-FH OFDMA under both cluster and independent hopping is plotted. The main objective of this example is to characterize the effects of frequency diversity exploited by RNS-FH patterns on system performance. Here, we assume that 10 users are in the system with 11 subcarriers assigned to each via the two-stage RNS hopping strategy. For cluster hopping, the moduli set used is $\{a_1 = 2, b_1 = 5\}$, while for independent hopping, it is $\{a_1 = 2, b_1 = 55\}$. It is observed that both independent and clustered RNS-FH OFDMA dramatically outperform the regular OFDMA scheme without hopping in both Veh A and Veh B environments. Another observation is that under both independent and cluster hopping, the system performs better in Veh A. That is, in the proposed RNS-FH patterns, large hopping intervals occur more frequently

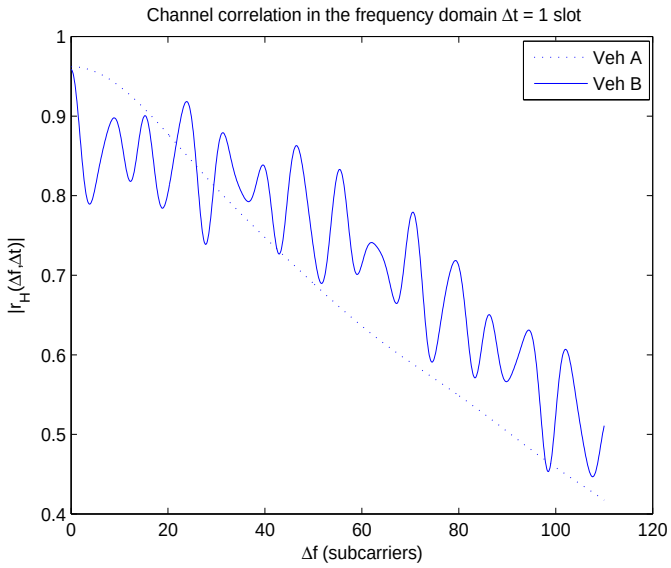

Figure 3.5: *Channel correlation function.*

than small hopping distances. This characteristic is very important since it reveals that users occupy a wide bandwidth during a small fraction of all hops. Furthermore, since independent hopping scheme results in a much larger FH pattern than cluster hopping, more frequency diversity can be exploited in the independent hopping case. This is also clearly reflected by the simulation results shown in Fig.3.7. For example, at a BER level of 10^{-3}, nearly 8dB gain is offered by independent hopping relative to cluster hopping in Veh A environment.

Fig.3.8 quantifies the inter-cell interferences experienced by different users in the cell of interest, averaged across time. The x-axis represents the indices of the users within the cell of interest while the y-axis characterizes the time-averaged inter-cell interference-to-signal power ratio for a given user. Two situations are considered: (1) different RNS-FH patterns are allocated to the cell of interest and the interfering cell (denoted by the solid line); (2) the same RNS-FH pattern as the cell of interest is assigned to the interfering cell (denoted by the dashed line). Here, we model the inter-cell interference as additive Gaussian distributed distortion. Therefore, in scenario (1), users in the cell of interest will

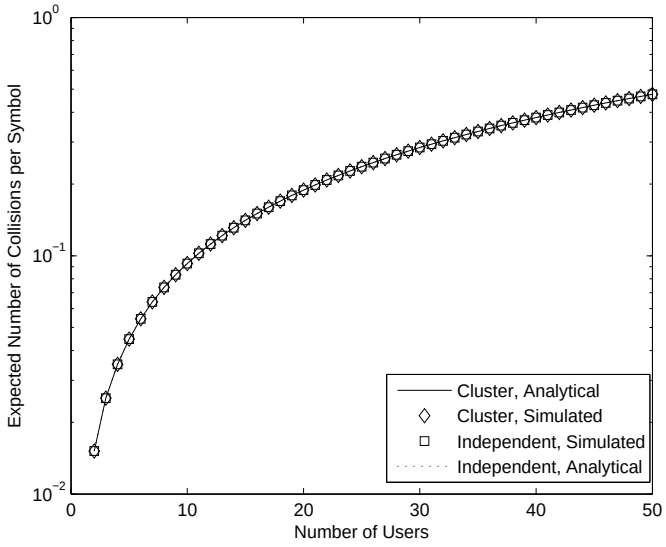

Figure 3.6: *Expected number of collisions per symbol versus the number of users.*

experience different interferences from the interfering cell across all hops, which in turn induces interference diversity. Fig.3.8 clearly demonstrates that by employing the proposed method (i.e., allocating a different RNS-FH pattern to the interfering cell), the inter-cell interference floor can be significantly lowered relative to the scenario where all cells employ identical RNS-FH patterns.

Fig.3.9 and 3.10 show the effects of inter-cell interference diversity on system performance. BER versus signal-to-interference ratio (SIR) is plotted under cluster and independent hopping in Fig.3.9 and 3.10, respectively. For cluster hopping, the FH pattern assigned to the interfering cell is constructed by using $\{a_2 = 5, b_2 = 2\}$ while it is $\{a_2 = 55, b_2 = 2\}$ for the independent hopping scenario. We simulate the case where the same RNS-FH pattern used in the cell of interest is assigned to adjacent interfering cells. Thus, users in the cell of interest will be affected by the same interferences from adjacent cells during all hops. Therefore, no interference diversity is exploited. Simulation results also reflect this feature. When the same RNS-FH pattern is assigned, frequency diversity as a result of hopping reduces the interference floor. Therefore the no hopping case still exhibits the worst BER perfor-

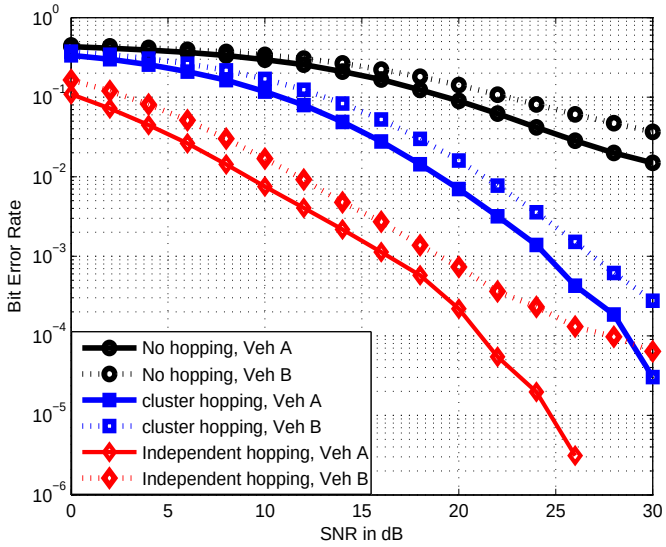

Figure 3.7: *BER vs. SNR of RNS-FH OFDMA under cluster and independent hopping with different channel conditions. N=110, M=M_c=10, N_c=11, f_DT_s=0.01.*

mance. When different patterns are allocated to interfering cells, the interference diversity along with frequency diversity further improves system BER performance. For example, in cluster hopping (Fig.3.9), with different pattern assignment, nearly 3dB gain at a BER level of 10^{-2} is achieved relative to the system employing identical hopping. This gain grows to 5dB under independent hopping scenario (Veh B environment).

BER versus user loads is plotted in Fig.3.11 and 3.12 under cluster and independent hopping respectively in both Veh A and Veh B. Effects of frequency and interference diversities on system performance are explored at given SNR and SIR. It is evident that the system throughput can be significantly enhanced by assigning different RNS-FH patterns to different cells, while it is severely limited if no hopping occurs. Furthermore, the performance gap between the identical hopping and the different hopping decreases with the increase in user loads. That is, the benefit of inter-cell interference diversity is greater for lower user loads.

Fig.3.13 illustrates that by increasing the cluster size (the number of subcarriers in one

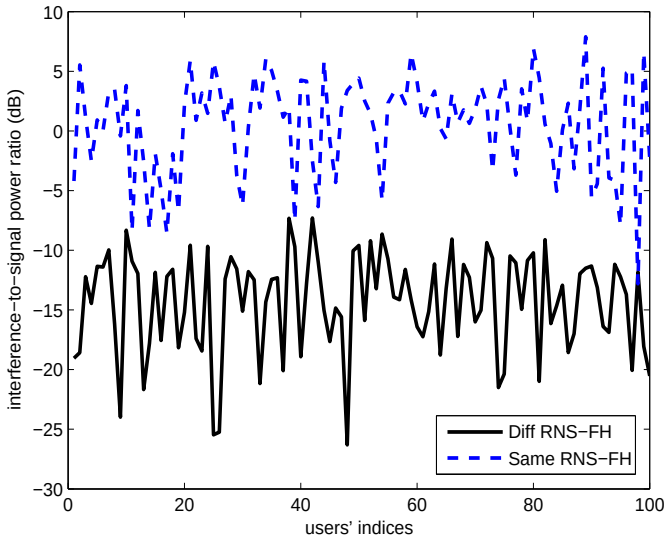

Figure 3.8: *Inter-cell interference-to-signal power ratio for given users under different RNS-FH patterns and identical RNS-FH patterns assignments across cells*

cluster), or the number of active users, the number of collisions increases. This in turn, induces degradation in BER performance as can be seen from Fig.3.13.

Finally, we compare our proposed RNS-FH pattern design strategy with state-of-the-art FH pattern designs. Specifically, our benchmark for comparison is the Latin Squares (LS) aided FH pattern design presented in [23]. In our proposed RNS-FH pattern, the spacing between hops in time and frequency is far enough that subcarriers employed in a single time slot are weakly correlated. This feature provides remarkable performance improvements that are consistent across all cells. However, in Latin Squares (LS) aided FH pattern design, performances in different cells may vary a lot. Relative comparisons are given in Fig.3.14, where two Latin Squares based FH patterns A_4 and A_{38} [23] are employed. In LS A_{38}, smaller hops happen more frequently, and for such smaller hops, Veh B exploits more frequency diversity than Veh A. The opposite is also true for LS A_4. Using simulation results, we first observe that in RNS aided FH-OFDMA, different RNS-FH patterns provide nearly the same BER performance, while it varies a lot in LS aided FH-OFDMA; the second

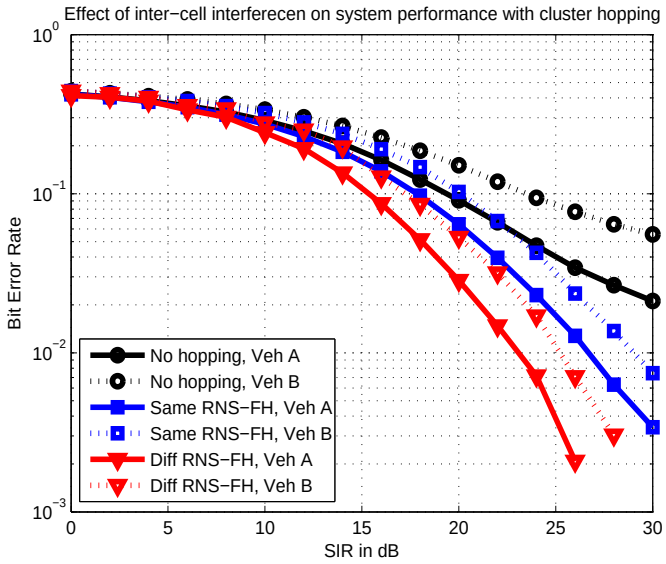

Figure 3.9: *BER vs. SIR of RNS-FH OFDMA under cluster hopping with different channel conditions. N=110, M=M_c=10, N_c=11, SNR = 25dB, $f_D T_s$=0.01.*

observation is that our proposed RNS-FH patterns have similar BER performances to LS A_4 while outperforming LS A_{38}. Although there may exist LS aided FH pattern that has better performance than the proposed scheme, the performance variations in LS aided FH pattern design really limit their applications.

3.4 Summery

In this chapter, we propose an RNS arithmetic based FH pattern design that is well suited and easy to implement for practical OFDMA cellular systems. RNS-FH patterns not only guarantee zero collision within a cell, but also average the inter-cell interferences by assigning different FH patterns to adjacent cells. Additionally, by having a large spacing between the hopping frequencies, the RNS-FH patterns exploit frequency diversity effectively and provide significant improvement in BER performance. The BER performance gain is consistent across all cells unlike other FH pattern design schemes such as the LS based method where

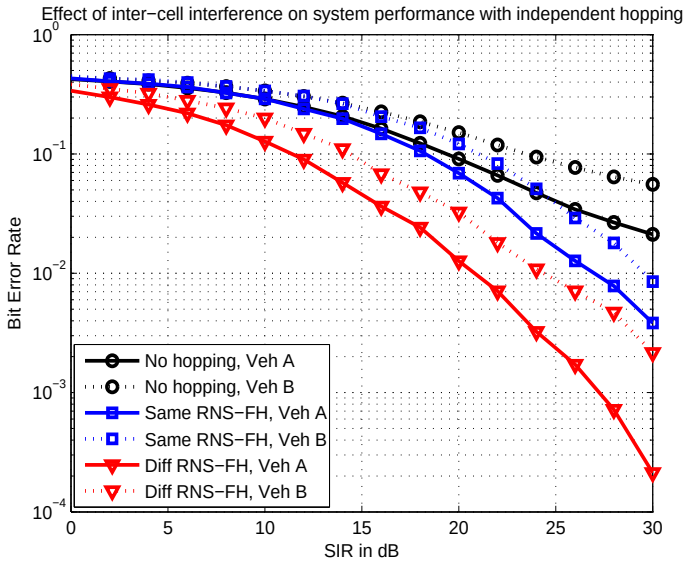

Figure 3.10: *BER vs. SIR of RNS-FH OFDMA under independent hopping with different channel conditions. N=110, M=M_c=10, N_c=11, SNR = 25dB, $f_D T_s$=0.01.*

wide performance variations are observed across cells. Simulation experiments demonstrate the superior performance of the RNS-FH scheme in terms of frequency diversity and inter-cell interference diversity under both independent and cluster hopping strategies.

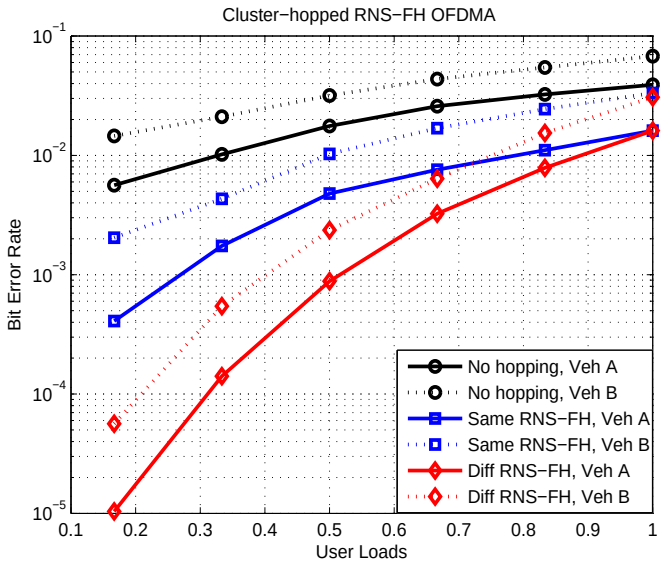

Figure 3.11: *BER vs. user loads of RNS-FH OFDMA under cluster hopping with different channel conditions, N=110, M=M_c=10, N_c=11, SNR = 25dB, SIR = 15dB, f_DT_s=0.01.*

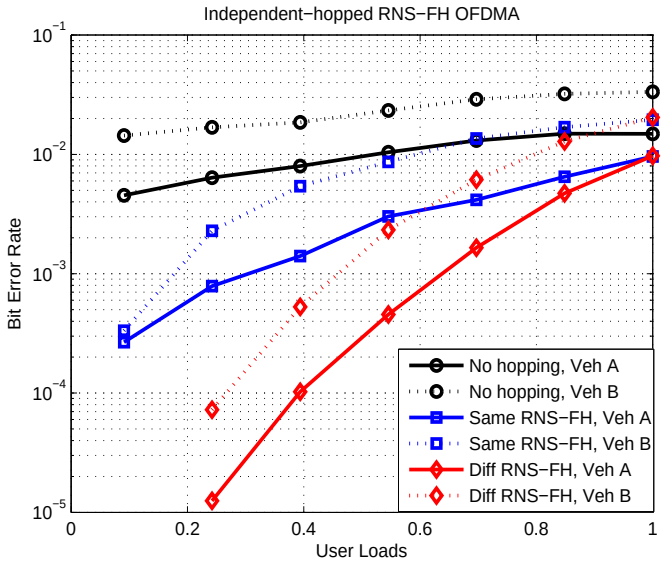

Figure 3.12: *BER vs. user loads of RNS-FH OFDMA under independent hopping with different channel conditions, N=110, M=M_c=10, N_c=11, SNR = 25dB, SIR = 15dB, f_DT_s=0.01.*

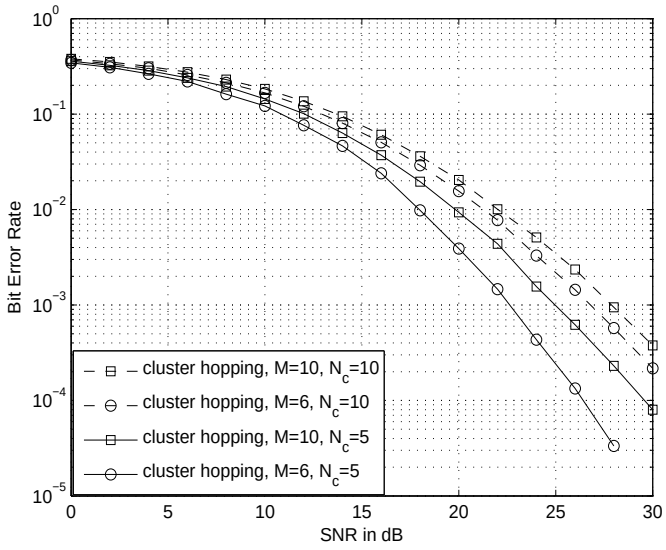

Figure 3.13: *Performance of cluster-hopped RNS-FH OFDMA with different cluster sizes and different number of active users,* $f_D T_s$*=0.01.*

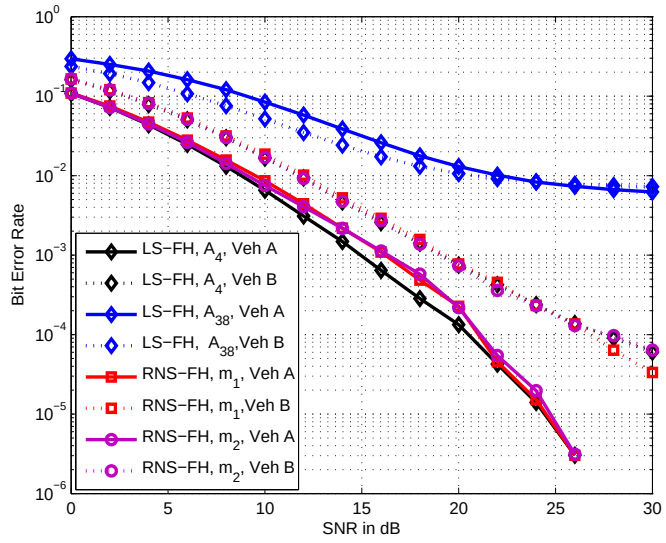

Figure 3.14: *Performance of independent-hopped RNS-FH OFDMA vs. LS-FH OFDMA,* N*=110,* M*=*M_c*=10,* N_c*=11, LS* A_4 *and* A_{38} *are used, different moduli sets* $m_1 = \{2, 55\}$ *and* $m_2 = \{2, 11, 5\}$ *are applied to construct RNS-FH patterns,* $f_D T_s$*=0.01.*

Chapter 4

RNS aided Pilot Pattern Design in Downlink OFDMA

In this chapter, we invoke the use of RNS to determine two-dimensional pilot patterns with limited mutual interference. The use of RNS in constructing a large set of multiple two-dimensional pilot patterns with low cross-correlation has not been investigated in any of the previous works in the literature. Therefore, understanding and quantifying the role of RNS in pilot assisted channel estimation in cellular OFDMA is the objective of this chapter.

4.1 System Model

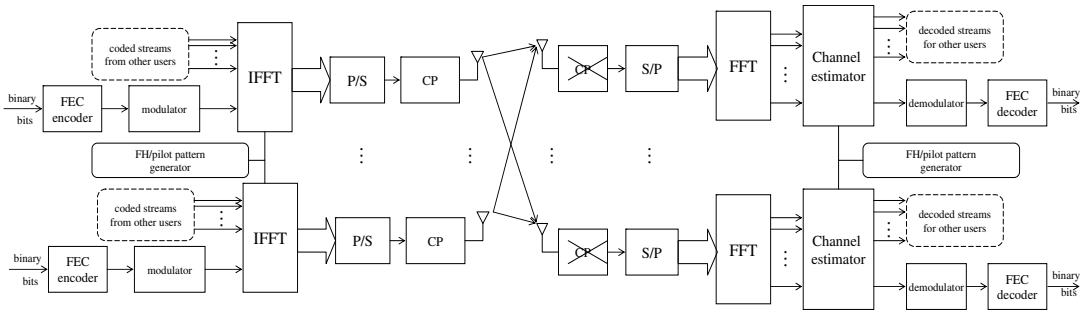

Figure 4.1: *Block diagram of MIMO-OFDMA system within a single cell*

The block diagram of a multi-antenna downlink OFDMA system in a single cell is given in Fig.4.1. M_t transmit antennas and M_r receive antennas are employed in the system. The number of subcarriers in one OFDM block per antenna is N, including N_c subcarriers as cyclic prefix (CP), and N_p subcarriers transmitting pilot signals. We further assume that there are N_u users in the system. Each user is assigned a specific set of subcarriers out of the total available subcarriers according to his/her data rates. Let $N_{i,m}$ be the number of subcarriers allocated to user i on the *m-th* transmit antenna. Then, user i's information symbols $\mathbf{x}^{i,m} = (x_1^{i,m}, x_2^{i,m}, \cdots, x_{N_{i,m}}^{i,m})^T$ ($(\cdot)^T$ represents the transpose operation) are transmitted on the assigned $N_{i,m}$ subcarriers. In this chapter, we introduce multiple antennas and pilot signals in the transmission scheme. Therefore, the corresponding mathematical model needs to be modified in contrast to that given in Chapter 3. The baseband transmitted signal for user i can be expressed as,

$$s^{i,m}(t) = \sum_{k=1}^{N_{i,m}} x_k^{i,m} e^{j2\pi \frac{k}{T_s} t}, 0 \leq t < T_s, \tag{4.1}$$

where, $s^{i,m}(t)$ represents the time domain signal and T_s denotes one OFDM symbol duration. Moreover, zeros are transmitted on subcarriers which are not assigned to user i. For convenience, we note $C_{i,m}$ as the subcarrier set that is assigned to user i on transmit antenna m. Hence, $N \times 1$ information symbols vector of user i can be written as

$$\mathbf{x}^{i,m}(k) = \begin{cases} 0, k \notin C_{i,m} \\ x_k^{i,m}, k \in C_{i,m} \end{cases}. \tag{4.2}$$

The discrete form of the transmitted signal $s^{i,m}(t)$ of user i is then given as,

$$\mathbf{s}^{i,m} = \mathbf{F}\mathbf{x}^{i,m}, \tag{4.3}$$

where $\mathbf{F}$ is the IFFT matrix defined as

$$\mathbf{F} = \frac{1}{\sqrt{N}} \begin{pmatrix} W_N^{00} & \cdots & W_N^{0(N-1)} \\ \vdots & \ddots & \vdots \\ W_N^{(N-1)0} & \cdots & W_N^{(N-1)(N-1)} \end{pmatrix} \tag{4.4}$$

where $W_N^{pq} = e^{j2\pi pq/N}$, $p, q = 0, 1, \cdots, N-1$.

Let $\mathbf{h}^{i,m} = [h^{i,m}(0), h^{i,m}(1), \cdots, h^{i,m}(N-1)]$ denote the discrete channel impulse response vector. The Fourier transform of the channel impulse response corresponds to

$$\mathbf{H}^{i,m} = \mathbf{F}^H \mathbf{h}^{i,m}, \tag{4.5}$$

where $(\cdot)^H$ represents the Hermitian transpose.

On the *n-th* receive antenna (after FFT), the received signal of user i on subcarrier k is

$$\mathbf{r}^{i,n}(k) = \sum_{m=1}^{M_t} \mathbf{x}^{i,m}(k)\mathbf{H}^{i,m}(k) + \mathbf{n}^{i,n}(k), \tag{4.6}$$

where $\mathbf{n}^{i,n}(k)$ is the Fourier transform of the additive Gaussian noise vector with mean 0, variance σ^2. Then, the overall received signal on the *n-th* receive antenna, *k-th* subcarrier is a superposition of signals transmitted for all N_u users, i.e.,

$$\mathbf{r}^{n}(k) = \sum_{i=1}^{N_u} \left[\sum_{m=1}^{M_t} \mathbf{x}^{i,m}(k)\mathbf{H}^{i,m}(k) + \mathbf{n}^{i,n}(k) \right]. \tag{4.7}$$

4.2 RNS-pilot Pattern Design

From the standpoint of sampling theory, in order to fully reconstruct the channel's delay-Doppler response, its time-frequency transform has to be sampled (at least) at Nyquist rates in both time and frequency domains. We can also interpret this in a broader sense. That is, in time domain, the sampling frequency $1/T_p$ should not be less than the channel's maximal Doppler spread $\nu_{\max}$, where T_p represents the spacing between two consecutive pilot probes in time. Similarly, in frequency domain, the sampling frequency $1/f_p$ must not be less than the channel's maximal delay spread $\tau_{\max}$, where f_p denotes the spacing between two consecutive pilot signals in frequency. In the context of OFDM, typical comb-type pilot patterns are widely used where pilot signals sample the channel's time-frequency response at Nyquist rates [52]. However, typical comb-type pilot pattern design lacks generality and this limits its application in identifying cells/devices, especially when the system is not time

synchronized. In this paper, we invoke the use of RNS to design equidistant two-dimensional pilot patterns with limited mutual interference. The resulting pilot signals not only sample the channel's time-frequency response at Nyquist rates, but also generate a much larger set of unique pilot patterns relative to regular comb-type and Costas array-based pilot patterns.

Following Nyquist sampling rates, assume G as the required number of OFDM symbols between two consecutive pilot signals in time, and M as the number of OFDM subcarriers between two consecutive pilots in frequency. Therefore, if T_s is one OFDM symbol duration and f is one subcarrier spacing, we have $T_p = GT_s$ and $f_p = Nf$. Based upon those assumptions, detailed design procedures of our proposed RNS-based pilot patterns are given as follows:

1. Partition the total available subcarriers N into M_c clusters with each cluster containing M number of contiguous subcarriers (i.e., $N = MM_c$).

2. If M can be written as a product of two pairwise relative primes, e.g., $M = a \times b$, then within each cluster, we can group a sub-clusters with b subcarriers in each sub-cluster.

3. Index the subcarriers in each sub-cluster from 0 to $b - 1$.

4. Index the sub-clusters in each cluster from 0 to $a - 1$.

5. At the 0-th time slot, assign integer N_k as the initial address (IA) of pilot signals, where $0 \leq N_k < M$.

6. If $N_k \text{mod}\{a, b\} = \{\hat{a}, \hat{b}\}$, then the $\hat{b}$-th subcarrier out of the $\hat{a}$-th sub-cluster is selected for transmitting pilot signal within one cluster.

7. Perform step 6 through all M_c clusters, M_c pilot signals are obtained with M OFDM subcarriers between each pair of the pilot signals.

8. At the t_s-th time slot, assign integer $N_k + t_s \text{mod}\{G\}$ as current address (CA) of pilot signals and repeat steps 6 - 7.

9. Repeat steps 6 - 8 until one mutually orthogonal pilot pattern is obtained.

10. If M can be expressed as products of w different combinations of two pairwise relative primes, then w different orthogonal pilot patterns can be obtained by repeating steps 2 - 9, w times.

One illustrative example of RNS-based pilot pattern design is given in Fig.4.2. In this example, we assume that $N = 12$, $M_c = 2$, $M = 6$ and $G = 4$. Straightforwardly, $M = 6 = 2 \times 3$. Therefore, if IA of pilot signals is 4, we have $4\text{mod}\{2, 3\} = \{0, 1\}$. This indicates that the 1-*st* subcarrier out of the 0-*th* sub-cluster within each single cluster is extracted out for transmitting pilot signals. This corresponds to the 2-*nd* and 8-*th* subcarrier in the 0-*th* OFDM symbol. At the 4-*th* time slot, the CA of pilot signals is calculated as $4 + 4\text{mod}\{4\} = 4$. In this time slot, same subcarriers as in the 0-*th* time slot are chosen for transmitting pilot signals (as can be seen from Fig.4.2). In general, the entire RNS-based pilot pattern is obtained by extending the generic $M \times G$ pilot pattern in both time (see dashed bi-directional arrow) and frequency (see solid bi-directional arrow).

It is worth noting here that property 1 (orthogonality property) of RNS sequences guarantees zero collision among pilot signals belonging to the same RNS-pilot pattern; property 2 of RNS sequences minimizes the number of pilot collisions among different pilot patterns. Here, we introduce another important property of RNS sequences that is associated with the application of RNS in constructing unique pilot patterns.

Property 3: If the system is perfectly time synchronized, the number of unique RNS sequences that are obtained from generic RNS-based pilot patterns is wMG^2. *Else, the number of unique RNS sequences is* wMG. □

Proof: The number of unique RNS sequences obtained via one $M \times G$ generic RNS-based pilot pattern is MG. Moreover, if IA/CA of pilot signals can be written as products of w different combinations of pairwise relative primes, wMG orthogonal RNS sequences are obtained. If time is perfectly synchronized, different time shifts of generic RNS sequences

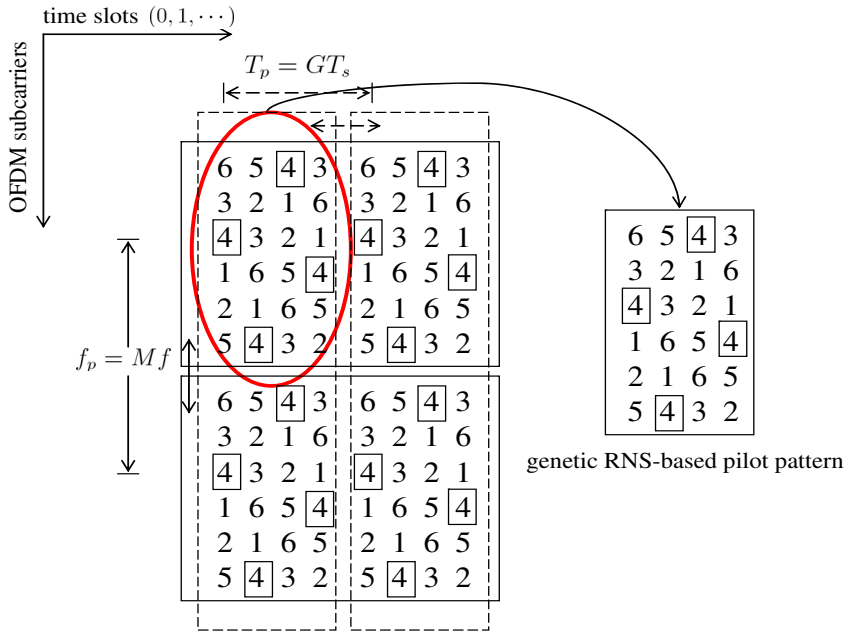

Figure 4.2: *Proposed RNS-based pilot pattern*

can also be taken into account. Under this scenario, the number of unique RNS sequences (and therefore, pilot patterns) is wMG^2. ■

In contrast to Costas array-based pilot pattern design and typical comb-type pilot patterns, where the number of unique pilot patterns is MG^2 and MG respectively (assuming perfect time synchronization), our proposed RNS-based method significantly enhances the degree of freedom for generating unique pilot patterns, especially when w is large. If multiple antennas are employed in each of the cells, orthogonal subsets of RNS-based pilot patterns can be allocated to different transmit antennas within the same cell. This will force intra-cell interference to zero. Alternately, different RNS-based pilot patterns are allocated to adjacent cells. In this way it is ensured that inter-cell interference can be well averaged.

Table 4.1: *System Parameters of pilot assisted OFDMA*

Transmission BW	5MHz
Carrier frequency	2GHz
OFDM symbol duration T_s	$100\mu s$
CP duration	$10\mu s$
Subcarrier spacing f	11KHz
FFT size	256
Occupied Subcarriers	240
Number of OFDM symbols per T (G)	6
Channel impulse response	6-ray UTRA
Channel coding	1/2 convolutional code
Modulation	QPSK
Number of interference cells	5
Number of transmit antenas M_t	2
Number of receive antennas M_r	1
Pilot power boost factor ρ [29]	0dB
Time Synchronization	Perfect

4.3 Simulation Results

Parameters of the simulated system is given in Table 4.1. The cyclic prefix within one OFDM symbol duration is assumed long enough to eliminate ISI (inter-symbol interference). 6-ray channel pulse response is considered following the UTRA Vehicular Test Environment [51]. Both link and system level performances are evaluated.

A. Link level performance

In Fig.4.3, symbol error rate (SER) performance of regular and RNS-based pilot pattern

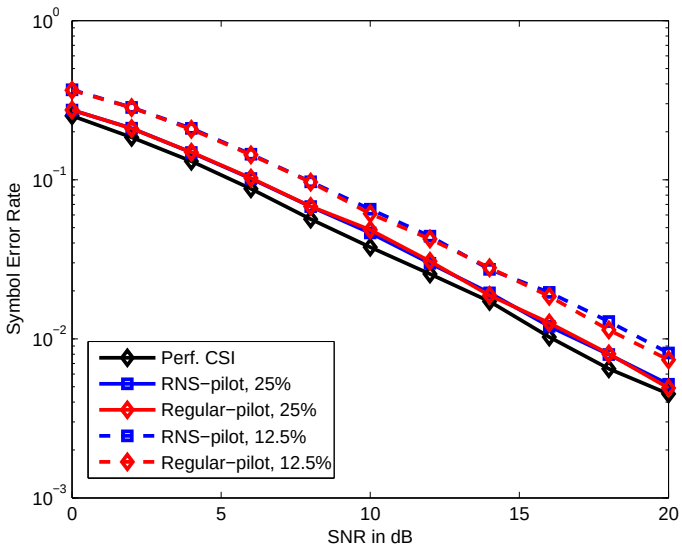

Figure 4.3: *SER performance of regular and RNS-based pilot pattern assisted channel estimation in a link level simulation, ρ=0dB*

aided Least Square (LS) channel estimation is evaluated. Various pilot densities are taken into account during the simulation, where the pilot density is defined as the ratio between the number of pilot signals and the total number of subcarriers. It is observed that under the same pilot density, RNS-based pilot pattern design is identical to regular comb-type pilot pattern in terms of SER. This is expected as the proposed RNS-based pilot pattern satisfies the sampling requirement (Nyquist rates) of typical two-dimensional pilot pattern design. Corresponding mean squared errors (MSEs) between estimated and actual channel realizations are simulated in Fig.4.4. Here, MSE is defined as

$$MSE = E[(\hat{\mathbf{h}}^{i,m} - \mathbf{h}^{i,m})^2], \tag{4.8}$$

where $\hat{\mathbf{h}}^{i,m}$ is the LS estimated channel response of actual $\mathbf{h}^{i,m}$. From Fig.4.4, we conclude that RNS-based method results in the same quality of channel estimation as compared to regular comb-type pilot pattern design.

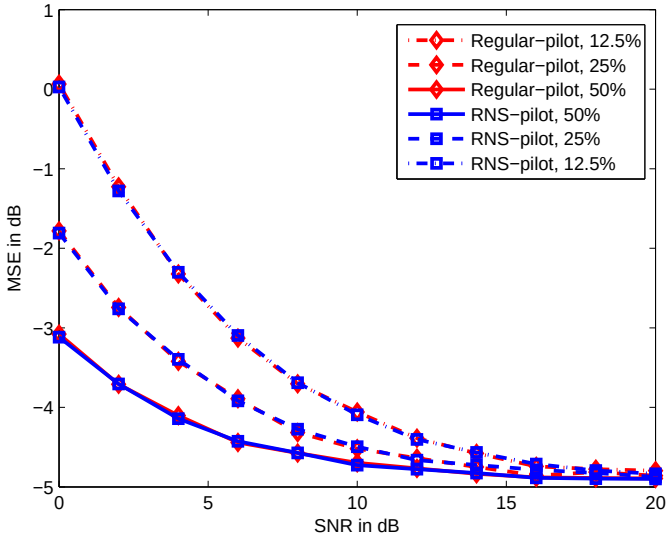

Figure 4.4: *MSEs of regular and RNS-based pilot pattern assisted channel estimation in a link level simulation, ρ=0dB*

Table 4.2: *Number of unique pilot patterns*

	No time syn.	Perf. time syn.
Regular pilot pattern	4	24
Costas-based pilot pattern	24	144
RNS-based pilot pattern	48	288

B. System level performance

Table 4.2 shows the number of unique pilot patterns that are generated using typical comb-type pilot pattern, Costas array-based pilot pattern and RNS-based pilot pattern. As demonstrated in section IV, RNS-based method can generate more unique pilot patterns than typical and Costas array-based pilot pattern design. Here, we assume $M = 4$ and $G = 6$. We further note that $w = 2$ as M can be written as $M = 1 \times 4 = 4 \times 1$.

In Fig.4.5, system throughput of RNS-based pilot pattern assisted OFDMA is plotted

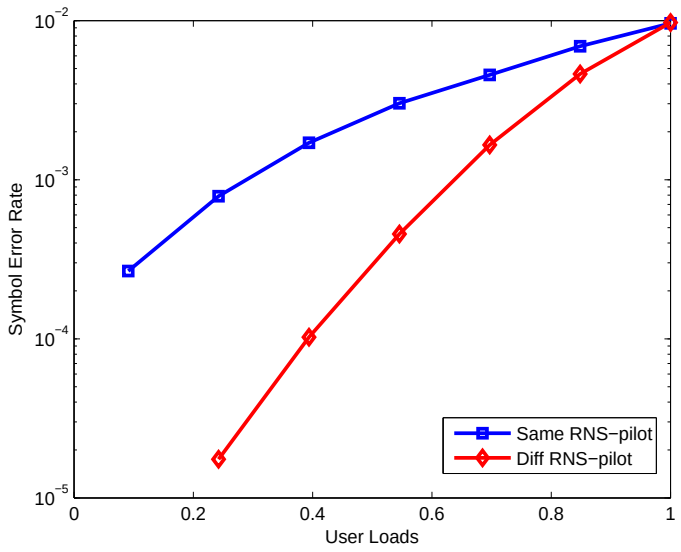

Figure 4.5: *System throughput of RNS-based pilot pattern assisted channel estimation in a system level simulation, SNR=20dB, SIR=15dB, ρ=0dB, 25% pilot density*

under fixed SNR and SIR values. Two scenarios are considered: (1) different RNS-based pilot patterns are assigned to the cell of interest and interfering cells; (2) same RNS-based pilot patterns are allocated to the cell of interest and interfering cells. As illustrated in section IV, pilot signals usually consume higher power comparing to data signals. Therefore, if same pilot patterns are employed in adjacent cells, pilot-to-pilot collisions severely degrade the quality of channel estimation and system throughput. We can also interpret this from the perspective of frequency reuse. That is, due to the inability to generate unique pilot patterns, comb-type and Costas array-based pilot patterns suffer from higher *adjacent channel interference* (due to pilot-to-pilot collisions) as compared to RNS-based approach. This in turn, results in worse throughput performance (as square line shown in Fig.4.5) in contrast to RNS-based method in a multi-cell environment.

4.4 Summary

In this chapter, a novel pilot pattern design method is proposed for downlink OFDMA. Specifically, residue number system arithmetic is used as a tool for constructing uniform pilot patterns with limited interference. In contrast to typical comb-type pilot patterns and Costas array-based approach, RNS-based method results in larger set of unique pilot patterns, which is extremely helpful for identifying user equipments (UEs) and enhancing system throughput.

Chapter 5

Conclusions and Future Work

So far, we have introduced two novel applications of residue number system arithmetic in cellular OFDMA systems, in Chapter 3 and 4, respectively. In this chapter, we give a comprehensive summary of our key contributions, along with suggestions on possible future work in this research area.

5.1 Conclusions

OFDM/OFDMA have been accepted as enabling techniques for next generation wireless communication systems. Residue number system (RNS) arithmetic has found widespread applications in both computer hardware design and communications. Hence, exploiting the use of RNS in practical OFDM/OFDMA systems becomes appealing, and is therefore, the main objective of this thesis. In our work, two important and interesting topics regarding OFDMA cellular systems are investigated. They are: (1) frequency hopping (FH) pattern design, and (2) efficient pilot pattern design. As a special case of linear congruence sequences, RNS has good properties, such as orthogonality and low cross-correlation, that are very helpful in constructing desired FH/pilot patterns for downlink OFDMA.

In Chapter 2, we start by giving brief introductions to conventional number system. Then, detailed descriptions of RNS arithmetic associated with its important properties are

shown. By comparing RNS with CNS, one can conclude that although RNS is less efficient to implement than CNS, as an integer number system, its good properties favor in both computer hardware design and communications.

Next, in Chapter 3, we propose a novel use of RNS in determining FH patterns for downlink OFDMA systems. Two strategies based upon RNS arithmetic are presented, which are: two-stage and multi-stage algorithm, respectively. Thanks to the orthogonality of RNS sequences and low cross-correlation among different RNS sequences, RNS-based FH patterns result in zero collision within the same cell, and minimization on symbol collisions between adjacent cells. Simulation results further justify our observations by showing superior BER and system throughput performances over existing schemes.

In Chapter 4, RNS arithmetic is involved in designing equidistant two-dimensional pilot patterns. We show that RNS-based approach has additional degrees of freedom in generating unique pilot patterns in contrast to conventional methods. This facilitates the identification process of user equipments in multi-cell multi-antenna environments. By using simulations, we further show that our proposed pilot patterns are identical to conventional methods in terms of SER from link level point of view. However, from a system level perspective, our proposed method results in better throughput performance.

5.2 Future Work

In our work, RNS-based FH pattern design in cellular downlink OFDMA has been well investigated from both theoretical and experimental perspectives. One interesting extension of this work is to apply RNS-based FH pattern to interleaved OFDMA. Interleaving is generally used in OFDMA. By combining interleaving and frequency hopping, additional frequency diversity gains can be exploited to further improve system BER performance.

In addition to channel estimation, RNS-based pilot patterns can aid in other synchronization tasks such as initial time-frequency offset estimation and device identification. The ambiguity function analysis frequently used in radar signal design leads to a periodic time-

hopping pattern based on the RNS sequence that has minimal coincidences with its circular time-frequency shifts, and can be used for the identification of multiple devices. The hopping in time also greatly increases the pilots' time support, thus enabling the quick initial acquisition of timing and frequency offset with very short observation. Investigating above mentioned aspects in the context of RNS-based pilot pattern design, will definitely be an interesting topic to explore.

In our work, the power boost factor ρ is set to be 0dB. Simply increasing the pilot power may not result in better quality of channel estimation. This is because under total power constraints, increasing the power of pilot signals will cause decrease in the power of actual transmitted signals. This in turn results in degradation in SNR at the receiver. Therefore, investigating the effect of changing the power boost factor on the quality of RNS-based channel estimation, or quantifying the corresponding trade-offs is also very interesting and important regarding practical concerns.

Bibliography

[1] R. W. Chang, "Synthesis of band-limited orthogonal signals for multichannel data transmission," in *Bell Systems Technical Journal*, vol. 46, Dec. 1966, pp. 1775–1796.

[2] S. B. Weinstein and P. M. Ebert, "Data transmission by frequency division multiplexing using the discrete fourier transform," in *IEEE Transactions on Communication Technology*, vol. com-19, Oct. 1971, pp. 628–634.

[3] H. Yin and S. Alamouti, "OFDMA: A broadband wireless access technology," in *IEEE Sarnoff Symposium*, Mar. 2006, pp. 1–4.

[4] L. Hanzo, M. Munster, B. J. Choi, and T. Keller, "OFDM *and* MC-CDMA *fro broadband multi-user communications,* WLANs *and broadcasting*," IEEE Press & Wiley, 2003.

[5] X. Li and L. J. Cimini, "Effects of clipping and filtering on the performance of OFDM," in *IEEE Communication Letters*, vol. 2, May 1998, pp. 131–133.

[6] S. Shepherd, P. van Eetvelt, C. Wyatt-Millingto, and S. Barton, "Simple coding scheme to reduce peak factor in QPSK multicarrier transmission schemes," in *Electronics Letters*, vol. 30, Jul. 1995, pp. 1131–1132.

[7] A. E. Jones, T. A. Wilkinson, and S. K. Barton, "Block coding scheme for reduction of peak to mean envelope power ratio of multicarrier transmission schemes," in *Electronics Letters*, vol. 30, Dec. 1994, pp. 2098–2099.

[8] D. Wulich, "Reduction of peak to mean ratio of multicarrier modulation by cyclic coding," in *Electronics Letters*, vol. 32, 1996, pp. 432–433.

[9] ——, "Peak factor in orthogonal multicarrier modulation with variable levels," in *Electronics Letters*, vol. 32, 1996, pp. 1859–1861.

[10] R. Dinis and A. Gusmao, "Performance evaluation of OFDM transmission with conventional and 2-branch combining power amplification schemes," in *IEEE Globecom*, Nov. 1996.

[11] D. Zhu and B. Natarajan, "Peak-to-average power ratio reduction in MIMO-OFDM with trellis exploration algorithm," in *proc. of IEEE International Conference on Computer Communications and Networks*, aug 2009.

[12] R. V. Nee and R. Prasad, "OFDM *for wireless multimedia communications*," Artech House Publishers, 1999.

[13] P. Moose, "A technique for orthogonal frequency division multiplexing frequency offset correction," in *IEEE Transactions on Communications*, vol. 42, Oct. 1994, pp. 2908–2914.

[14] M. Sandell, J. J. van de Beek, and P. Borjesson, "Timing and frequency synchronization in ofdm systems using the cyclic prefix," in *International Symposium on Synchronization*, Dec. 1995, pp. 16–19.

[15] W. Warner and C. Leung, "OFDM/FM frame synchronization for mobile radio data communication," in *IEEE Transactions on Vehicular Technology*, vol. 42, Aug. 1993, pp. 302–313.

[16] H. Sari, G. Karam, and I. Jeanclaude, "Transmission techniques for digital terrestrial TV broadcasting," in *IEEE Communications Magazine*, Feb. 1995, pp. 100–109.

[17] T. J. Kahwa and N. Georganas, "A hybrid channel assignment scheme in large scale cellular structured mobile communication systems," in *IEEE Transactions on Communications*, vol. com 26, 1978, pp. 432–438.

[18] D. Cox and D. Reudink, "Increasing channel occupancy in large scale mobile radio systems: dynamic channel reassignment," in *IEEE Transactions on Communications*, vol. 21, 1973, pp. 1302–1306.

[19] M. K. Simon, J. K. Omura, R. A. Scoltz, and B. K. Levitt, "Spread spectrum communications," Computer Science Press, Rockville, Md, USA, 1985.

[20] T. Scholand, T. Faber, A. Seebene, J. Lee, J. Cho, Y. Cho, H. W. Lee, and P. Jung, "Fast frequency hopping OFDM concepts," in *Electronics Letters*, vol. 41, no. 13, Jun. 2005.

[21] T. Kurt and H. Delic, "On symbol collision in FH-OFDMA," in *IEEE Vehicular Technology Conference*, vol. 4, no. 13, May 2004, pp. 1859–1863.

[22] ——, "Space-frequency coding reduces the collision rate in FH-OFDMA," in *IEEE Transaction on Wireless Communications*, vol. 4, no. 5, Sep. 2005.

[23] K. Stamatiou and J. G. Proakis, "A performance analysis of coded frequency-hopped OFDMA," in *Proceeding of IEEE WCNC*, Mar. 2005.

[24] S. V. Maric and M. O, "Using costas arrays to construct frequency hop patterns for OFDM wireless systems," in *Conference on information sciences and systems*, Mar. 2006, pp. 505–507.

[25] C. Wang, X. Zhang, and D. Yang, "Evaluation of Welch-Costas frequency hopping pattern for OFDM cellular system," in *IEEE International Symposium on PIMRC'07*, Sep. 2007, pp. 1–5.

[26] T. Li, Q. Ling, and J. Ren, "A spectrally efficient frequency hopping system," in *IEEE Globecom'07*, Nov. 2007, pp. 2997–3001.

[27] B. M. Popovic and Y. Li, "Frequency-hopping pilot pattern for OFDM cellular systems," in *IEICE Trans. Fundamentals*, vol. E89-A, no. 9, Sep. 2006.

[28] J. C. Guey, "Synchronization signal design for OFDM based on time-frequency hopping patterns," in *IEEE conference on communications*, Jun. 2007, pp. 4329–4334.

[29] A. Osseiran and J. C. Guey, "Hopping pilot pattern for interference mitigation in OFDM," in *IEEE PIMRC 2008*, Sep. 2008, pp. 1–5.

[30] "Identification of a base station, using latin-square hopping sequences, in multicarrier spread-spectrum systems," in *European Patent Application EP 1-148-673-A3*, Oct. 2001.

[31] B. M. Popovic and Y. Li, "Frequency-hopping pilot patterns for OFDM cellular systems," in *IEICE Trans. Fundamentals.*, vol. E89-A, no. 9, Sep. 2006, pp. 2322–2328.

[32] D. Zhu and B. Natarajan, "Residue number system arithmetic assisted coded frequency-hopped OFDMA," in *EURASIP Journal on Wireless Communications and Networking*, vol. 2009, Article ID 263695, 11 pages, doi:10.1155/2009/263695.

[33] ——, "Residue number system arithmetic aided freuquency-hopping pattern design in coded OFDMA," in *proc. of IEEE Vehicular Technology Conference 2009-Fall.*

[34] ——, "Residue number system arithmetic inspired pilot pattern design in downlink OFDMA," in *submitted to IEEE International Conference on Communications, 2010.*

[35] G. H. Andrews, "*Number Theory*," Dover Publications, 1st Ed., 1994.

[36] A. Omondi and B. Premkumar, "*Residue Number System: Theory and Implementation*," Imperial College Press, 2007.

[37] F. J. Taylor, "Residue arithmetic: A tutorial with examples," in *IEEE Transactions on Computers*, vol. 17, no. 5, May 1984, pp. 50–63.

[38] A. Sasaki, "The basis for implementation of additive operations in the residue number systems," in *IEEE Transactions on Computers*, vol. C-17, Nov. 1968, pp. 1066–1073.

[39] T. R. N. Rao and A. K. Trehan, "Binary logic for residue arithmetic using magnitude index," in *IEEE Transactions on Computers*, vol. C-19, Aug. 1970, pp. 752–757.

[40] M. A. Soderstrand and R. A. Escott, "VLSI implementation in multiple-valued logic of an FIR digital filter using residue number system arithmetic," in *IEEE Transactions on Circuits and Systems*, vol. 33, Jan. 1986, pp. 5– 25.

[41] R. W. Watson and C. W. Hastings, "Self-checked computation using residue arithmetic," in *Proceedings of the IEEE*, vol. 54, Dec. 1966, pp. 1920– 1931.

[42] F. Barsi and P. Maestrini, "Error correcting properties of redundant residue number systems," in *IEEE Press*, 1986, pp. 352–360.

[43] M. H. Etzel and W. K. Jenkins, "Redundant residue number systems for error detection and correction in digital filters," in *IEEE Transactions on Acoustics, Speech, and Signal Processing*, vol. 28, Oct. 1980, pp. 538–545.

[44] L. Hanzo, L. L. Yang, E. L. Kuan, and K. Yen, "*Single- and multi-carrier* DS-CDMA*: multi-user detection, space-time spreading, synchronization and standards*," John Wiley & Sons Ltd, 2003.

[45] H. Krishna, K. Y. Lin, and J. D. Sun, "A coding theory approach to error control in redundant residue number systems - Part I: theory and single error correction," in *IEEE Transactions on Circuits and Systems*, vol. 39, Jan. 1992, pp. 8–17.

[46] J. D. Sun and H. Krishna, "A coding theory approach to error control in redundant residue number systems - Part II: multiple error detection and correction," in *IEEE Transactions on Circuits and Systems*, vol. 39, Jan. 1992, pp. 18–34.

[47] H. Krishna and J. D. Sun, "On theory and fast algorithms for error correction in residue number system product codes," in *IEEE Transactions on Computer*, vol. 42, Jun. 1993, pp. 840–852.

[48] L. Bin, "One-coincidence sequences with specified distance between adjacent symbols for frequency-hopping multiple access," in *IEEE Transactions on Circuits and Systems*, vol. 39, Jan. 1992, pp. 18–34.

[49] A. Lempel and H. Greenberger, "Families of sequences with optimum Hamming correlation properties," in *IEEE Transactions on Information Theory*, vol. 20, 1974, pp. 90–94.

[50] J. G. Proakis, "*Digital Communications*," Mc Graw Hill, 4th Ed., 2001.

[51] *ETSI TR 101 112, UMTS 30.03, V3.1.0, Annex B, Std.*

[52] S. Coleri, M. Ergen, A. Puri, and A. Bahai, "Channel estimation techniques based on pilot arrangement in OFDM systems," in *IEEE Transactions on Broadcasting*, vol. 48, Sep. 2002, pp. 223–229.